ABSTRACT

DEVELOPMENT OF AN EXPERIMENTAL SYSTEM TO DETERMINE THE CONTRIBUTION OF TITIN AND COLLAGEN TO PASSIVE STIFFNESS OF MYOCARDIUM

by
Saurin Bharat Shah

Diastolic dysfunction is known to be a major factor for congestive heart failure in aged humans and other mammals. The main contributors to increase in the myocardial stiffness, hindering the cardiac mechanics, are alterations in intracellular titin and extracellular collagen matrix. Titin is a giant extensible protein, the third filament of striated muscle after actin and myosin, which provides elasticity to passive sarcomeres. The aim of this study is to develop an efficient experimental system that will prove to be instrumental in comparing the contribution of titin against collagen to the passive stiffness of cardiac muscle extracted from experimental animals of different age groups. To accomplish a reliable technique, a pool of sophisticated devices like piezoelectric translation stage, force transducer and high speed video sarcomere length measurement system was assembled to function in coordination with each other. In addition, protocols were written to perform controlled experiments on the cardiac muscle specimen under consideration. To verify the sustainability and repeatability of the system, heart tissue from rats and pigs were used to perform trials and acquire data. From the trials conducted using myocardium of adult (but not senescent) animals, the recorded data was found to follow trends anticipated from published literature for non-aged myocardium. These findings suggest the system will also be able to satisfactorily conduct repeated experiments with aged myocardium.

DEVELOPMENT OF AN EXPERIMENTAL SYSTEM TO DETERMINE THE CONTRIBUTION OF TITIN AND COLLAGEN TO PASSIVE STIFFNESS OF MYOCARDIUM

by
Saurin Bharat Shah

A Thesis
Submitted to the Faculty of
New Jersey Institute of Technology
in Partial Fulfillment of the Requirements for the Degree of
Master of Science in Biomedical Engineering

Department of Biomedical Engineering

May 2009

Blank Page

APPROVAL PAGE

DEVELOPMENT OF AN EXPERIMENTAL SYSTEM TO DETERMINE THE CONTRIBUTION OF TITIN AND COLLAGEN TO PASSIVE STIFFNESS OF MYOCARDIUM

Saurin Bharat Shah

_5/21/09_

Dr. William C. Hunter, Thesis Advisor Date
Professor of Biomedical Engineering, NJIT

_5/21/09_

Dr. William C. Van Buskirk, Committee Member Date
Distinguished Professor of Biomedical Engineering, NJIT

_5/21/09_

Dr. Sergei Adamovich, Committee Member Date
Assistant Professor of Biomedical Engineering, NJIT

BIOGRAPHICAL SKETCH

Author: Saurin Bharat Shah

Degree: Master of Science

Date: May 2009

Undergraduate and Graduate Education:

- Master of Science in Biomedical Engineering,
  New Jersey Institute of Technology, New Jersey, USA, 2009

- Bachelor of Engineering (Hons.) Electronics and Instrumentation
  Engineering,
  Birla Institute of Technology and Science, Dubai, UAE, 2007

Major: Biomedical Engineering

To my parents for all their blessings, my sister for the inspiration and all my friends for always being there.

This would have never been possible without the support and encouragement of one and all.

"The World is an awesome place, but I am better off Engineering it."
Saurin Shah

ACKNOWLEDGMENT

TABLE OF CONTENTS

TABLE OF CONTENTS
(Continued)

TABLE OF CONTENTS
(Continued)

TABLE OF CONTENTS
(Continued)

TABLE OF CONTENTS
(Continued)

LIST OF TABLES

LIST OF FIGURES

LIST OF FIGURES
(Continued)

LIST OF FIGURES
(Continued)

CHAPTER 1

INTRODUCTION

1.1 Overview

Congestive heart failure becomes a major problem when it comes to morbidity and mortality associated with increase in age [1]. The contribution of diastolic dysfunction to such age-related heart failure is significant when compared to other factors. The elastic properties of heart tissue, that stiffen the left ventricular chamber and elevate late-diastolic pressure, are the most detrimental of all the mechanisms that could possibly lead to diastolic dysfunction [2].

Alterations in the myocardium contributing to such elevated chamber stiffness could arise due to changes in both the intracellular fibrillar protein titin and the extracellular collagen matrix. The main purpose of this thesis was to develop an experimental system that will enable tests to elucidate the individual roles of titin versus collagen in passive (diastolic) elasticity of cardiac muscle strips from old versus young mammals.

The current hypothesis is that the extracellular contribution to stiffness increases with age mainly due to alterations in the collagen matrix. On the other hand, the sarcomeric contribution to stiffness (from titin) may decrease with age due to expression of a different protein isoform of titin. For moderate stretch, these opposing changes tend to cancel out one another when the left ventricle operates in its compliant region. However, in case of longer stretch, the functional change in the collagen matrix with increased age dominates and

1

decreases the upper limit of passive stretch. This hypothesis is supported by preliminary biochemical data, but there have been no mechanical tests to substantiate the same.

The objective at hand demands a thorough knowledge of passive cardiac mechanics, which includes structure and function of passive myocardium and a thorough understanding of the sarcomeric protein titin and the interstitial collagen matrix. The initial chapters of the thesis will discuss these two areas of interest. Moreover, to enable practical experimental tests of the hypothesis, a highly sophisticated experimental setup had to be designed and assembled from devices with high precision and accuracy. The later chapters report the development of this system which will then enable experimental trials to acquire valuable data related to the passive stiffness of the heart in old versus young mammals.

1.2 Background Studies

As mentioned earlier, recent studies indicate that one major cause of congestive heart failure is abnormal diastolic function, and this is increasingly a common reason for morbidity and mortality upon aging [3, 4]. Clinical studies estimate that 50% of all congestive heart failure patients above the age of 70 suffer from diastolic dysfunction rather than systolic failure. The left ventricle of a heart that is suffering from diastolic dysfunction ejects nearly normal stroke volume at close to normal ejection fraction, thereby enabling an end diastolic volume that is not

greatly expanded. Nevertheless, filling the left ventricle to such nearly normal volumes in these patients requires significantly elevated end-diastolic pressure.

In a more recent review [2] it has been suggested that the likely source for elevated late diastolic pressure in patients with diastolic dysfunction are changes in the intra sarcomeric protein network and the extracellular collagen fibrous network. Kass et al. mention that other mechanisms – such as delayed relaxation, actively maintained diastolic tone, and extrinsic forces – are less likely to contribute to elevated late diastolic pressures in chronic diastolic heart failure [2].

Many researchers have affirmed that the elevation of risk factors for diastolic heart failure increase with age [5-7]. As quoted from Lakatta's paper [7], "A fundamental understanding of age associated changes in cardiovascular structure and function ranging in scope from humans to molecules is required for effective and efficient prevention and treatment of cardiovascular disease in older persons."

Changes in the extracellular collagen matrix can certainly affect diastolic function [8]. The myocardial collagen matrix is composed of three major constituents, (1) fibrillar proteins such as the collagen types I and III and elastin, (2) proteoglycans, and (3) basement membrane proteins such as collagen type IV, laminin and fibronectin. Amongst all these the contribution of fibrillar collagen to diastolic myocardial stiffness is likely to be the most important, especially with larger stretch of diastolic myocardium.

Apart from the extracellular collagen matrix, cytoskeletal changes could also contribute to diastolic dysfunction. In case of myocytes, a network of proteins that constitutes its cytoskeleton is responsible for determining the passive elastic behavior of the cell. In cardiac myocytes the cytoskeleton is composed of actin (microfilaments), desmin (intermediate filaments), and α and β tubulin that form microtubules by polymerization. All these together form the extra-sarcomeric cytoskeleton of the cardiac myocyte. This network is ensnared with the sarcomeric lattice composed of the endosarcomeric proteins actin, myosin, titin, nebulin, α-actinin, myomesin and M-protein. Of these, titin and desmin contribute most to the diastolic elastic behavior of myocytes [9].

In the mammalian genome, there is only one gene coding for titin. Nevertheless, differential splicing results in at least two isomers of titin that are expressed simultaneously in cardiac muscle [10, 11]. They are named N2B and N2BA titin isoforms [10]. These will be discussed in depth in chapter 3. A variation in proportions of each isoform in a cell leads to a strikingly different passive stress-strain behavior when performing passive stiffness tests on a muscle strip in the myofilament direction. Thus changes in titin isoform composition in cardiac myocytes are likely to modulate the diastolic stiffness of the myocardium [10, 12-14]. However, not much is known with certainty about age-related alterations in titin isoforms either in humans or other mammals.

Aging is also known to change the extracellular collagen matrix of the heart [15]. Increase in age may alter the relative content of Type I collagen in comparison to Type III collagen in the myocardium. Some studies suggest

increase in ratio of Type I collagen to Type III collagen with age while some others suggest a decrease in same [16]. In addition to this, collagen does not turn over rapidly in myocardium, although slowly, collagen does turn over and its total mass in the heart is regulated by a balance between synthesis and degradation [17, 18]. Unpublished data from research at the University of Medicine and Dentistry of New Jersey, Newark, NJ suggest alterations in these processes with age result in net change in total amount of collagen present per myocardial tissue volume. The other factor that changes the stiffness of collagen matrix is the nature and degree of cross-links between its fibrils [19-21]. In humans and other mammals, collagen often becomes glycated over time and increased numbers of advanced glycation end-products (AGEs) are expected to increase with age, which lead to an increase in cross-links between collagen fibrils. This is also suggested to be a likely mechanism for age-related increase in myocardial stiffness [22-27]. However, the functional impact of these changes on the elastic behavior of the collagen matrix in heart has not been quantitatively analyzed.

1.3 The Objective

The main aim of this thesis is to design and develop an experimental system viable to perform repeat experiments that would quantitatively investigate the contribution of the intracellular protein titin against the extracellular collagen matrix to the passive stiffness of myocardium and its changes with increase in age.

While developing the experimental setup, the study shall also build a reliable technique to avail stress-strain data on the passive stiffness of heart with individual contributions of titin and collagen to the same. Furthermore, the design of the system shall be such that the same experimental system could be utilized for the study of active stresses in the myocardium with just minor alterations to the setup designed to measure the passive stiffness of heart.

CHAPTER 2

SARCOMERE SERIAL AND PARALLEL ORGANIZATION WITHIN A

CARDIAC MYOCYTE

2.1 The Cardiac Myocyte

Myocardium is that layer of the heart wall that accounts for the contraction and expansion mechanism of the heart during the pumping process. The myocardium is composed of cardiac muscle cells or myocytes. These myocytes are built up of sarcomeres, the spring action of which causes the heart to contract or expand during the systolic and diastolic process of the heart. These units are held together by the Z-disks. The alignment of these disks is handled by a component in the cytoskeleton of the heart that runs in the transverse direction, and which is extended across the cell membrane into the extracellular matrix at specific sites called costameres.
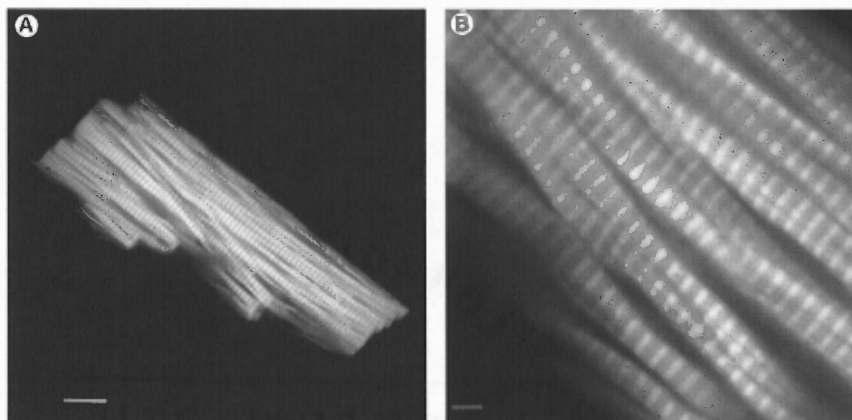
Figure 2.1 Orientation of Sarcomeres. A) Parallel to the Long Axis of Cardiac Myocyte, B) Along the Myofibrils.
Source: Z. Su, A. Yao, I. Zubair, K. Sugishita, M. Ritter, F. Li, J. J. Hunter, K. R. Chien, and W. H. Barry, "Effects of deletion of muscle LIM protein on myocyte function," *Am J Physiol Heart Circ Physiol,* vol. 280, pp. H2665-2673, 2001.

2.2 Sarcomeres

A sarcomere is the fundamental structural unit of cardiac myocytes and any other striated muscle cell. The passive elastic properties of sarcomeres shall be presented in the next chapter. The major proteins present in a sarcomere are actin, myosin and titin. The sarcomeres are responsible for the contraction and expansion of the myocardium when signaled to do so. It is a prime contributor to the stiffness of myocardium.

As seen in figure 2.1, sarcomeres form a highly organized serial and parallel array inside a cardiac myocyte. The serial array of sarcomeres is formed into the myofibrils that often run from one end to the other in a myocyte. If we observe closely, the myofibrils remain in register in figure 2.1. This implies that the bonding pattern remains matched amongst all the parallel myofibrils across the cell.

The Z-discs connect sarcomeres from end to end along the length of the myofibril. The Z-disc, as the locus of cross-links between thin filaments in successive sarcomeres, serves to transmit the force generated by myofilaments along the myofibril. The Z-disc also forms an integral part of the transverse cytoskeleton of the myocyte.

2.3 Transverse Cytoskeleton of Myocytes

The transverse cytoskeleton links the Z-discs in neighboring sarcomere with each other and thereby aligns the Z-discs going across the cell. This structure, mainly composed of desmin, provides both transverse and shear stiffness to the

myocyte and thus maintains the integral structure of the myocytes while successfully undergoing repeated expansion and compression cycles. When the transverse cytoskeleton reaches the outer limit of the cell (sarcolemma) then a special structure connects the transverse network across and into the next cell. These structures are known as costameres (see figure 2.2). Costameres are subsarcolemmal protein assemblies that circumferentially align in register with the Z-disk of peripheral myofibrils and physically couple force-generating sarcomeres with the sarcolemma in striated muscle cells [28].
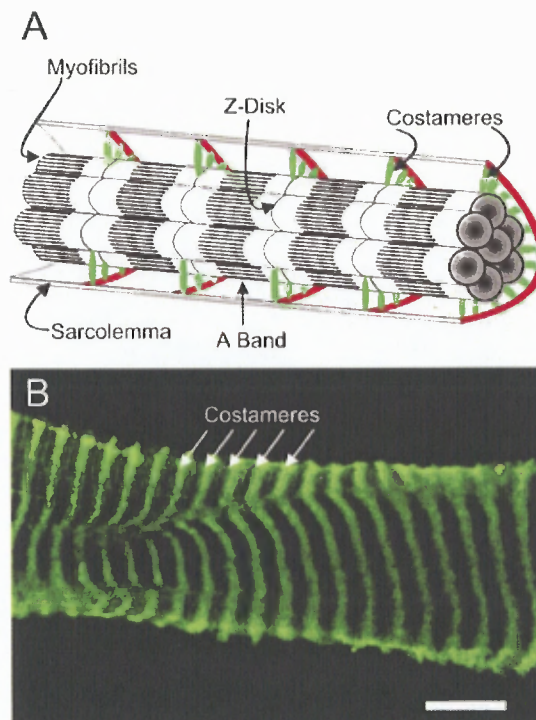
Figure 2.2 Cellular Locations of Costameres in Striated Muscle. Shown in A is a schematic diagram illustrating costameres as circumferential elements that physically couple peripheral myofibrils to the sarcolemma in periodic register with the Z-disk. Shown in B is an inside-out sarcolemma that was mechanically peeled from a single myofiber.
Source: J. M. Ervasti, "Costameres: the Achilles' Heel of Herculean Muscle," *J. Biol. Chem.,* vol. 278, pp. 13591-13594, 2003.

CHAPTER 3

STRUCTURE AND FUNCTION OF TITIN

3.1 About Titin

Titin, also known as connectin, is a sarcomeric protein found in both skeletal and cardiac muscle. This giant elastic protein is the third filament of striated muscle after actin and myosin [29]. The molecules of titin span from Z-disc to the M-line region at the center of the sarcomere. A large part of titin is extensible which enables it to function as a modular spring and maintain precise structural arrangement of thin and thick filaments [30].

Titin is the largest known natural protein composed of a single amino acid chain. It has a length greater than 1μm and weighs approximately 3MDa [31]. Apart from this, it also has the longest IUPAC name with 189,819 letters, which is sometimes considered to be the longest word in the English language. The chemical formula of titin is:

$$C_{132983}H_{211861}N_{36149}O_{40883}S_{693}$$
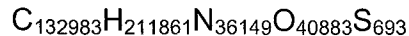
Although early studies of striated muscle, when subjected to over stretching, revealed the presence of additional filaments along with the thick filaments, it was not until 1980s that these filaments were uniquely identified as titin. The modern understanding of structure and function of the sarcomeric titin, present in the heart muscle, is a result of the extensive studies conducted during the late 1980s that explained the structure and detailed arrangement of titin in the

sarcomere [29]. Titin constitutes 10% of sarcomeric protein, the third most abundant after myosin (40%) and actin (22%).

Functionally, titin grants elasticity to the sarcomere and thereby generates passive elastic recoil forces when a sarcomere is stretched beyond its resting, unstressed length [32]. During the diastolic phase of the cardiac cycle, the myocardium expands, stretches cardiac myocytes, and generates a passive force. Titin is the major contributor to this passive force developed within each myocyte. It is also a major determinant of the passive stiffness of heart [10]. Prior to the delineation of the functional role of titin, collagen alone was believed to be the primary contributor to the passive stiffness of cardiac muscle [29].

Recent research also suggests that the role of titin goes beyond the generation of passive stiffness. During systole, titin may adjust actomyosin interaction by a titin-based alteration of the distance between myosin heads and actin. Furthermore, unique ligands have been recognized that bind to titin and interact with membrane channels, protein turnover, and gene expression [13].

3.2 Structure of Titin

Titin is the largest known mammalian protein. Depending on the isoform composition, this protein ranges from 2970 to 3700 kDa [29]. Human titin is encoded by a single gene that contains 363 exons (see figure 3.1). Exons 1 to 251 are Z-disc and I-band exons, 116 of which are PEVK (proline[P], glutamate[E], valine[V] and lysine[K] residues) exons and the rest are serially linked immunoglobulin like domains also known as the tandem Ig segment. The

A-band region of titin is encoded by exons 252 to 363. Exon 358 codes for a

serine-threonine kinase domain with unknown physiological function [30].
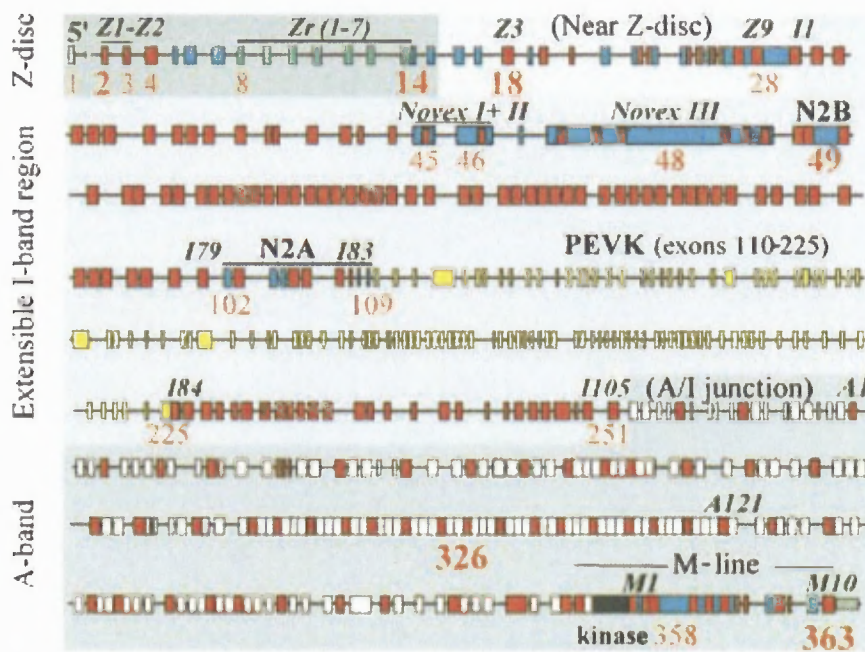
Figure 3.1 Exon-intron Structure of Human Titin Gene.
Source: H. L. Granzier and S. Labeit, "The Giant Protein Titin: A Major Player in Myocardial Mechanics, Signaling, and Disease," Circ Res, vol. 94, pp. 284-295, 2004.

Investigating further into the I-band encoding region of the titin gene, the

multiple splice pathways give rise to isoforms with distinct elastic compositions.

Exon 49, which contains the N2B sequence, is not present in skeletal muscle

titin, but is present in all cardiac titin isoforms. Splicing of exons 49/50 to exon

219 results in the small cardiac isoform known as N2B titin. A second class of

cardiac isoforms, in addition to the N2B element, also contains exons 102 to 109

(coding for the N2A element), the so-called N2BA titin isoform. N2BA titins have

a longer PEVK segment and contain additional Ig domains (see figure 3.2) [33]. It

is said that increase in N2B isoform content elevates the passive stiffness of heart while N2BA, being compliant, reduces the cardiac passive stiffness.
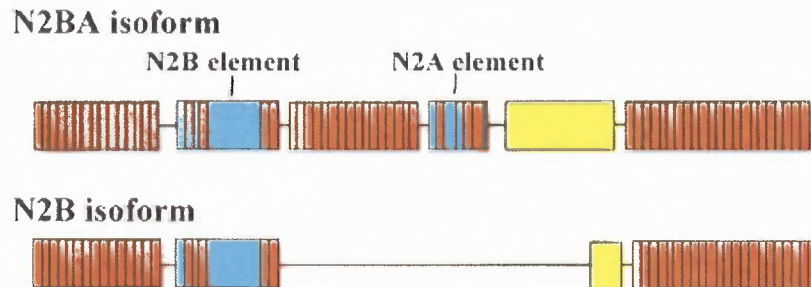
Figure 3.2 Domain Structure of Extensible I-band Region of Cardiac Isoforms. In red are the Ig domains.
Source: H. L. Granzier and S. Labeit, "The Giant Protein Titin: A Major Player in Myocardial Mechanics, Signaling, and Disease," Circ Res, vol. 94, pp. 284-295, 2004.

Titin is an integral part of sarcomere. Its N-terminus is attached to the Z-disk and the protein extends to the M-line region of the sarcomere, where it is bound to the myosin rod. An inextensible region near the Z-disk segment in the I-band is bound to the thin filament [29].
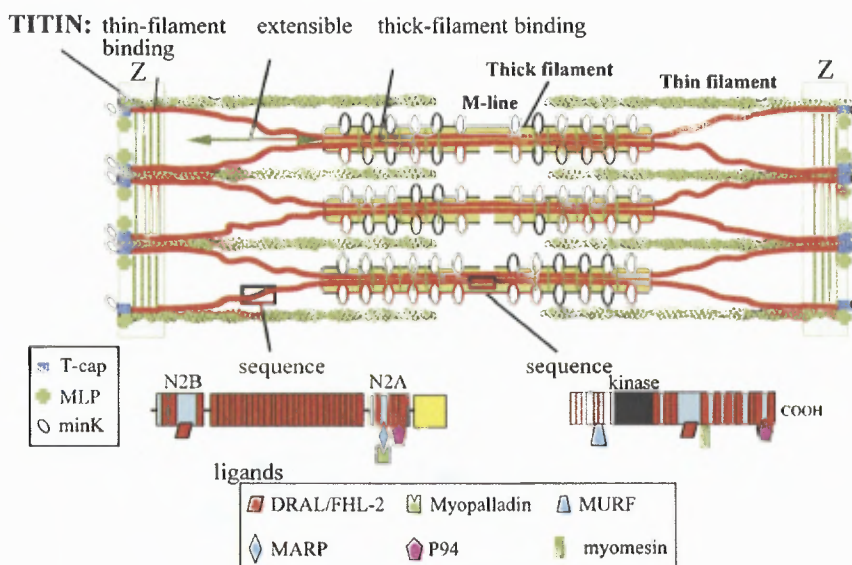
Figure 3.3 Position and Structure of Titin within the Sarcomere.
Source: M. M. LeWinter, Y. Wu, S. Labeit, and H. Granzier, "Cardiac titin: Structure, functions and role in disease," *Clinica Chimica Acta,* vol. 375, pp. 1-9, 2007.

3.3   The Modular Spring Nature of Titin

When passive striated muscle is stretched, titin is the myofilament that develops

the passive force. The titin related force is mainly generated by an extensible

segment located in the I-band region of the sarcomere. As mentioned earlier, this

extensible region is composed of proximal tandem Ig segments near the the Z-

line and distal tandem Ig segments near the A-band. Both these segments are

separated by the PEVK domain, yet another extensible region of titin in the

I-band [34].
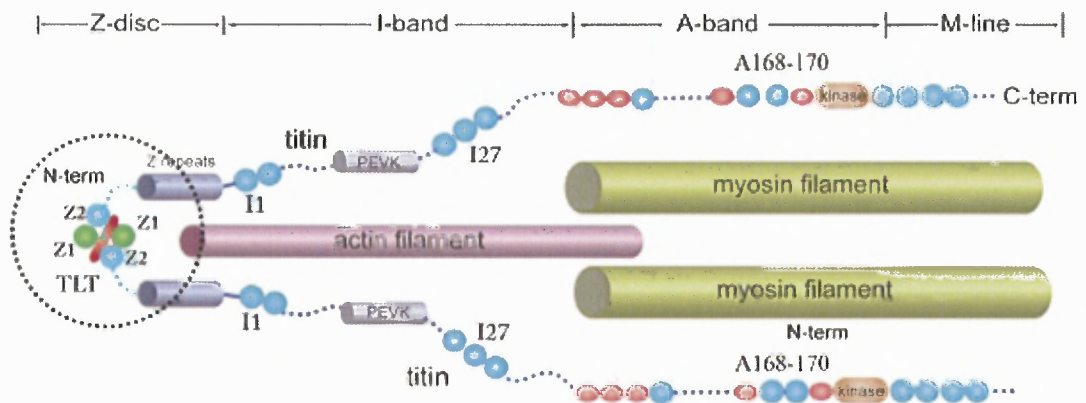
Figure 3.4 Schematic View of Titin. The N-terminal of titin is anchored to the Z-disk and the C-terminal to the M-line.
Source: E. H. Lee, J. Hsin, O. Mayans, and K. Schulten, "Secondary and Tertiary Structure Elasticity of Titin Z1Z2 and a Titin Chain Model," *Biophys. J.,* vol. 93, pp. 1719-1735, 2007.

The behavior of titin during passive stretching of sarcomeres was

explained thoroughly by the results obtained from immuno-electronmicroscopic

experiments performed with antibodies to various epitopes. In the absence of

external forces, the I-band region of titin is highly folded, with a near zero end-to-

end length. With stretch, much of the I-band segment gradually lengthens and

functions as a spring, developing passive tension. In contrast, the A-band region of titin is inextensible [29].

The spring nature of the elements of titin during stretching is complex. The tandem Ig segments extend before PEVK and N2B/N2A segments. This gives rise to distinct segments of the cardiomyocyte passive tension–sarcomere length relation, which is shallow near slack length but much steeper at longer sarcomere lengths. With contraction of the sarcomere below slack length the thick filament moves into the near Z-disk region of titin. As a result, the extensible region is stretched in the opposite direction as that during passive elongation and a restoring force is established that pushes the Z-disks away from each other during relaxation. Thus, titin functions as a bidirectional spring and accounts for the bulk of the restoring force responsible for cardiac myocyte recoil after unloaded contraction [29].

3.4 Function of Titin in Passive Cardiac Myocyte Mechanics

Until mid 1990s very less research had been conducted to recognize the source of this passive tension when compared with active tension, which is based on actomyosin interaction. Since the diastolic wall tension is the prime determinant of the extent to which the heart can be filled, the passive tension is an important factor in cardiac muscle. Hence now studies are more focused to clearly identify the passive tension aspect of the heart and titin's role in them [35].
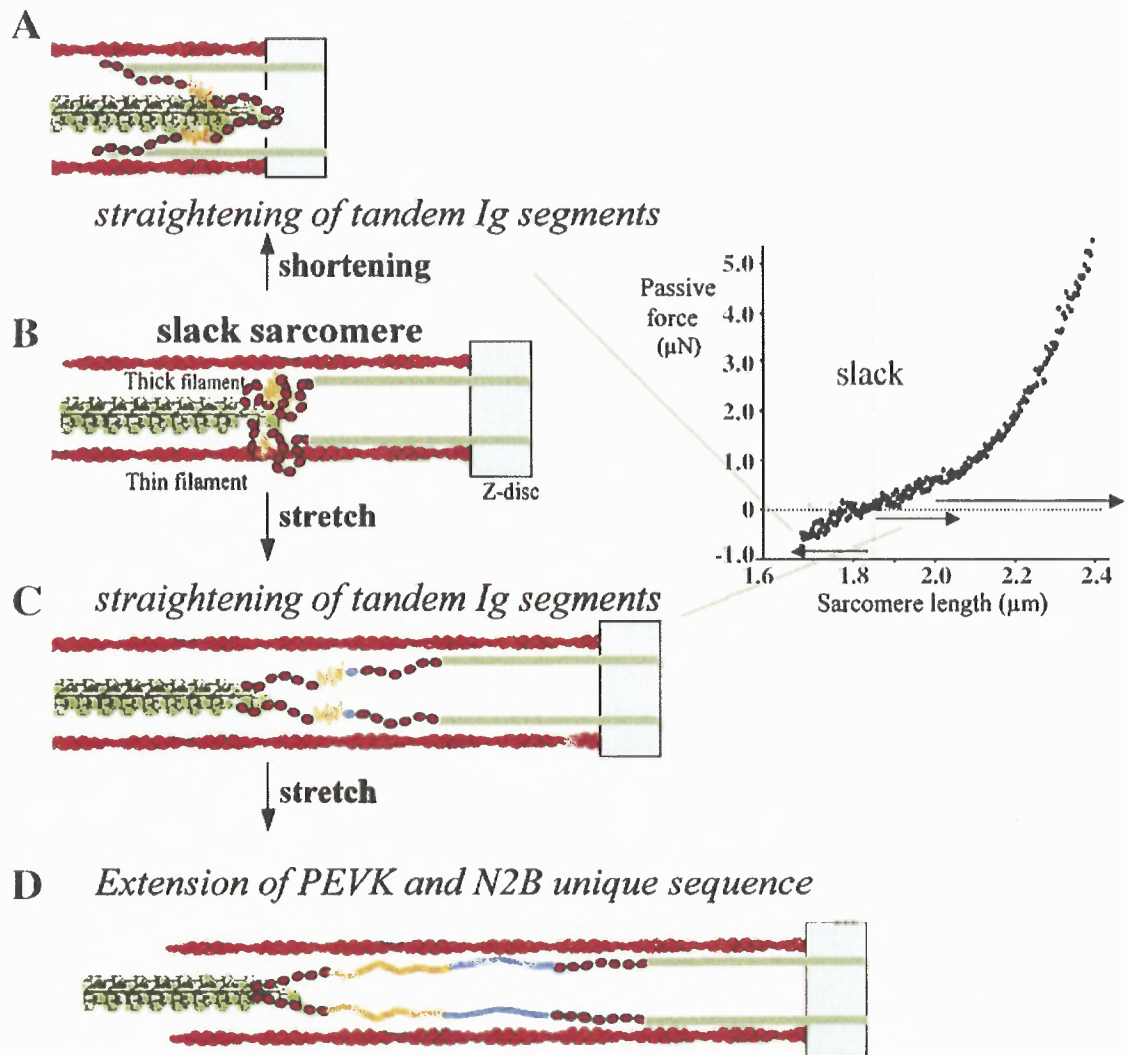
Figure 3.5 Titin as Modular Spring. Stretching of the sarcomere from slack length (panel B) results in sequential extension of tandem Ig (panel C) and then PEVK and N2B elements (panel C), each of which is responsible for a segment of the sarcomere length (SL)–passive force relation (right). Shortening below slack length (panel A) results in reverse extension of titin with development of a restoring force.
Source: M. M. LeWinter, Y. Wu, S. Labeit, and H. Granzier, "Cardiac titin: Structure, functions and role in disease," Clinica Chimica Acta, vol. 375, pp. 1-9, 2007.

The extensible region of titin described in the previous sections largely accounts for the passive force in cardiac myocytes during sarcomere stretch. As mentioned earlier, this extensible region spans from near Z disk to the edge of the A band. Being highly flexible, the extensible region, in absence of external force shortens to a near zero length due to the thermally driven bending motions. This results in a reduction of conformational entropy that gives rise to the passive force. It is this passive force that pulls the Z-disks towards each other [30].

The segments that constitute the titin's extensible region have unique bending rigidities. As a result, sarcomere stretch sequentially leads to the extension of the tandem Ig segments followed by extension of PEVK and N2B segments. The cardiac specific N2B segment is known as N2B – Unique sequence (N2B-Us). The extension of N2B-Us lowers the passive force levels, which in turn makes the complete unfolding of Ig domain unlikely and reduces energy loss due to repeated unfolding and refolding with the progression of cardiac cycles [30].

The passive force hysteresis in stretch-release cycles expresses that the passive myocytes display the property of viscoelasticity. As per the research conducted by Granzier and Labeit, the underlying mechanisms in cardiac myocyte specific viscoelasticity may involve dynamic interaction between actin and titin, dynamic cross-links in PEVK and N2B-Us regions and unfolding of Ig domains [30]. The exact basis of titin's viscoelasticity is yet to be determined.

Titin, as stated earlier, is essential for sustaining the structural integrity of the sarcomere. Titin's passive force offers resistance to sarcomere stretch and

paired with collagen, it determines the upper limit of physiological sarcomere length. Titin's restoring force sets the lower sarcomere length limit during systolic cycle of heart function, thereby being an important determinant of diastolic filling.

3.5 Role Played by Titin in Pathophysiology

Several studies conducted in the past have reported the association of alteration in titin expression with diastolic dysfunction. Research undertaken by Granzier and Labeit, based on canine tachycardia-induced model of dilated cardiomyopathy, explains the response of titin to chronic mechanical challenge of heart [30]. The rapid pacing in this model increases chamber stiffness and chamber dilation [36]. Consequently, elevated N2B titin expression and down regulation of N2BA titin have been recorded as results for the same study [30]. This implies that there is an increased N2B-N2BA ratio, thereby, expressing the elevation of titin based passive stiffness in tachycardia-induced cardiomyopathy [29, 34].

In another study by Nagueh et al, patients with dilated cardiomyopathy were segregated, based on the diastolic filling patterns, into impaired relaxation, pseudonormal and restricted filling sub groups. Conclusively, the study suggested that restricted diastolic filling has the highest N2B-N2BA ratio, followed by pseudonormal and impaired relaxation filling patterns [37].

On similar lines, studies have also shown that, in contrast to dilated cardiomyopathy, mitral regurgitation has increased N2BA expression. This decreases the N2B-N2BA ratio resulting in increased compliance of the heart

muscles when an individual suffers from mitral regurgitation [34]. In another study conducted by Neagoe reveals that the N2B-N2BA ratio in donor hearts with a background of coronary artery disease is lesser than that of normal hearts [38].

Apart from the above mentioned acquired titin diseases, titin, due to its enormous size and diverse functions, is susceptible to mutations, thereby, giving rise to muscle disease. Investigations involving sequencing the entire titin gene in dilated cardiomyopathy families unveiled mutations in exons 18 and 326 of the titin gene. A truncated titin is what results due to the frame shift caused to mutation in exon 326 [30]. A separate study recognized two mutations in exons 2 and 14 in patients suffering from hypertrophic cardiomyopathy [29].

CHAPTER 4

STRUCTURE AND FUNCTION OF MYOCARDIAL COLLAGEN

4.1 About Collagen

The term collagen is used to name a family of proteins present in extracellular locations and providing important role in the biology of tissues. In other words, collagen is a type of fibrous protein that connects and supports bodily tissues, such as skin, bone, tendons, muscles, and cartilage [15]. It also supports the internal organs and is even present in teeth. There are more than 25 types of collagens that naturally occur in the body, of which collagen type I, III, IV and V are found in the extracellular matrix of the heart. The interstitial collagens, types I and III are the most abundant components [17]. Collagen is one of the most plentiful proteins present in the human body. It makes up about 25 percent of the total amount of proteins in the body. Collagen fibers are thus the major contributors to the mechanical stiffness of the extracellular matrix in the myocardium [15].

Collagen is present in the form of long polypeptide chains called α-chain that associate to form a triple helix. These structures aggregate and form a collagen fibril which is visible in the electron microscope. Fibril diameters vary from tissue to tissue (25–80 nm). Clusters of these fibrils associate to form the collagen fiber bundles which are visible by light microscopy [15].

Studies have proved that collagen is in reality a family of various different protein molecules. Based on the composition and arrangement of α-chains in

20

collagen molecules, more than 25 types of collagen have been identified, as mentioned earlier. The various types of collagen have a different chemical structure, morphology, distribution, functional structure, and pathology [15, 17].

Of all the known types of collagen, the collagen type I, II, III, V and XI form fibrils, while the rest are loosely described as non-fibrillar. Collagen type I is mainly distributed in the organs, tendons, dermis, bone, fibrous cartilage and dentine. Collagen type II is present mainly in cartilage. Type III is predominantly abundant in the uterus, arteries and muscle. Collagen type IV is present in basal laminae [39].

Functionally, collagen type I provides elastic resistance to stress in tissues that work under tension (such as cardiac muscle), collagen type II offer resistance to intermittent pressure in tissues that work under compression (such as articular cartilage), while collagen type III provides structural connectivity in expansible organs. Collagen type IV acts to anchor layers holding groups of cells together [40].

4.2 Structure of Myocardial Collagen

Anatomical observations have shown that the cardiac tissue has a highly specialized architecture. As mentioned in chapter 2, the structure is composed primarily of cardiac muscle cells, or myocytes, arranged in a more or less parallel weave called muscle fibers [41].

The interstitium of the myocardium contains a ground substance that comprises of glycosaminoglycans and glycoproteins, blood vessels, nerves and

connective tissue [42]. Connective tissue consists predominantly of collagen, and to a much lesser extent, fibronectin, laminin, and elastic fibers. The diversity of the components of the connective tissue of cardiac muscle undoubtedly reflects the considerable dynamic requirements of the heart as it undergoes dramatic changes in shape during the cardiac cycle [43].

Structurally, there are three components of the collagen network which are the epimysium, perimysium and endomysium (see figure 4.1) [44]. The epimysium is the connective tissue sheath surrounding the entire muscle, the endomysium surrounds individual myocardial cells, and the perimysium surrounds groups of myocytes [43].
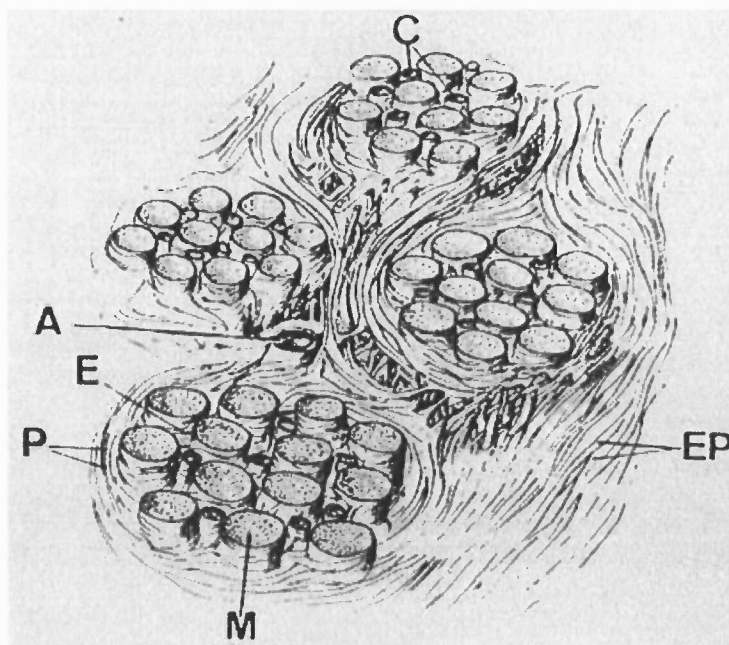
Figure 4.1 Schematic Representation of the Myocardial Collagen Network. EP – epimysium; P – perimysium; E – endomysium; M – myocyte; A – arteriole; C – capillaries.
Source: R. R. De Souza, "Aging of myocardial collagen," Biogerontology, vol. 3, pp. 325-335, 2002.

Studies conducted by Borg et al. on the connective tissue of mammalian heart muscle gives a detailed description of the extracellular structures and their arrangement relative to cardiac muscle cells (see figure 4.2). Each muscle fiber is surrounded by a sheath of connective tissue (epimysium). This sheath contains a large number of collagen fibers and far fewer elastin fibers. Observations on papillary muscle show a regular geometrical arrangement of this sheath in the form of a crisscross weave. Such a network could protect the sarcomere from overstretching [45]. When the fiber is stretched to sarcomere lengths between 2.3 and 2.5µm, the collagen fibers are essentially aligned along the axis and the muscle fiber, thus providing a structure more resistant to deformation [46].

The connective tissue is also composed of struts formed by bundles of collagen fibrils (endomysium) that interconnect adjacent muscle fibers. These struts have a diameter ranging between 120 and 150 nm [45]. They appear to be quite slack in the stress-free state and are aligned primarily transverse to the muscle fiber direction, but branch in quite random directions before attachment to adjacent myoctes. This hierarchy of branching structures leads to an essentially isotropic component to the heart structure [41].
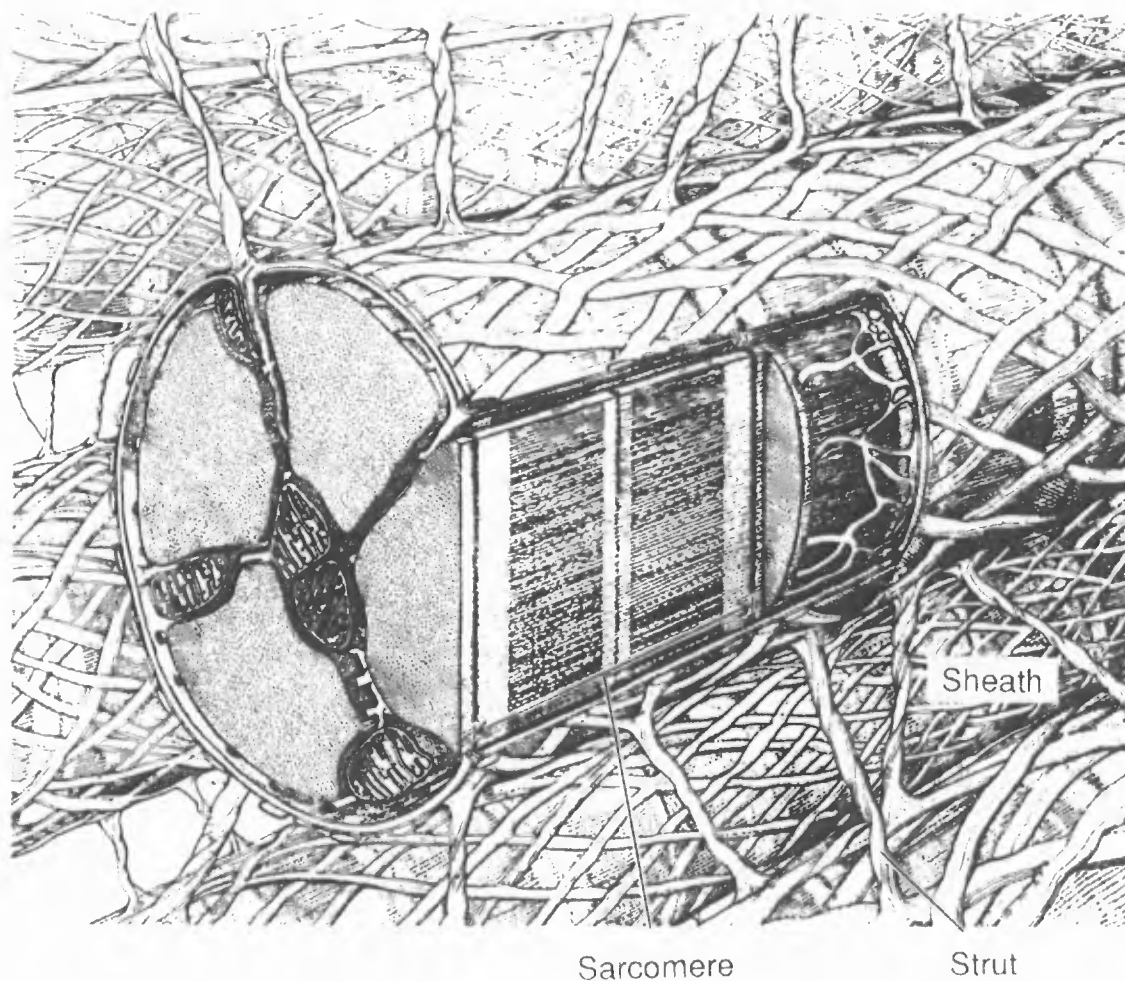
Figure 4.2 Schematic View of the Microstructure of the Endomysial Collagen. The sheath surrounding myocytes and the collagen struts interconnecting neighboring myocytes are shown in this figure.
Source: J. Ohayon and R. Chadwick, "Effects of collagen microstructure on the mechanics of the left ventricle," Biophysical Journal, vol. 54, pp. 1077-1088, 1988.

4.3 Function of Myocardial Collagen

Collagen is a vital component of the extracellular matrix of both the heart and blood vessel walls. It acts as a scaffold to maintain myocardial shape and permit an even distribution of force while playing a crucial role in the mechanical properties of the blood vessels and myocardium [47]. In the myocardium, the interstitial collagen matrix surrounds and supports cardiac myocytes and the coronary microcirculation [46, 48]. Owing to the tensile strength and arrangement in a network, surrounding and inter-connecting myocytes and capillaries, these collagens transmit forces throughout the myocardium, maintain cardiac structure during the cardiac cycle and contribute to the visco-elastic properties of the myocardium [17]. In addition, the interstitial collagen, 1) functions as a medium between myocytes and the circulatory and lymphatic systems through which electrolytes, macromolecules, oxygen and metabolic waste products must diffuse; 2) serves as an important determinant of ventricular diastolic function and ventricular size and 3) coordinates the transmittal of forces generated by myocytes to the ventricular chamber [49].

The collagen fibers in ventricular myocardium contribute to the tensile stiffness of the wall, especially at larger cavity volumes, while maintaining the structure of myocytes and myofiber bundles. Large coiled perimysial collagen fibers provide tensile stiffness, whereas smaller endomysial fibers surrounding and interconnecting individual myocytes prevent myocyte slippage and maintain unloaded ventricular geometry [50]. Specifically, myocardial collagen is the basis

for myocardial diastolic stiffness and protects myocytes from being overstretched [49].

4.4 Myocardial Collagen as a Function of Age

Aging results in the progressive decline of the cardiovascular system, characterized in part by an increase in wall thickness of the ventricles due to the alterations in the extracellular matrix of the myocardium. Aged humans and other mammals experience ventricular hypertrophy associated with an excess accumulation of the fibrillar protein collagen, a major structural component of the cardiac extracellular matrix [51].

Collagen in many organs of the body, including tendons, muscle, the liver and the lung changes with age. The solubility of collagen when heated to 65^0C decreases. Similarly, contraction in the body produces higher tensions in the tendons of the aged. An increase in cross links of the collagen macromolecules occurs with aging. The total collagen content in many tissues has been found to increase with age, a condition referred to as fibrosis [15]. In addition, ratio of collagen type I to type III may also increase with age in the myocardium. This indicates that more of the collagen is present in the thicker, stiffer fibers.

CHAPTER 5

DESIGN RATIONALE

The development of any system requires a valid design developed to meet technical criteria. Thus the right design rationale was very crucial for the successful realization of an efficient and reliable experimental system. This chapter lays down the fundamental criteria for the particular design we adopted as base for the development of the experimental system.

5.1 The Objective – Revisited

Before jumping into designing the system we would like to reiterate the objective of this thesis, which is development of an experimental system to determine the contribution of titin against collagen to the passive stiffness of myocardium. The aim here was to create a setup to artificially generate passive stresses in the test specimen, which as originally conceived, could vary from a single cell myocyte to a multi-cellular myocardium preparation. The generated stress levels would be in close approximation to those generated during the natural cardiac cycle.

The specified goal not only involves generation of passive stresses in the myocardial specimen but also development of a technique to investigate, using the same experimental set up, the contribution of titin versus collagen to the passive stiffness of the heart. In order to achieve distinct data on the individual contribution of titin and collagen to the passive stresses, first, the passive force generated by the cardiac muscle strip under test was to be recorded without any

special treatment. This would give us the combined contribution of both titin and collagen to the passive stiffness of the specimen. Followed by this, the cardiac muscle strip would be treated with solutions that depolymerize thick and thin filaments in order to remove titin's anchor point on the thick filament, thereby, eliminating its effect on any kind of muscle mechanics. The same mechanical stretch experiment would now be performed on the cardiac muscle strip in which titin plays no role. In this way we get data that would display contribution of collagen only to the passive stiffness of the myocardium strip; published results suggest that there is no effect of the depolymerizing solutions we used on the collagen matrix [35]. The difference in the two available stress-strain data would produce the effect of titin alone on the passive stiffness of the cardiac muscle strip.

In addition, the investigative procedure was to be based on uniaxial loading and unloading, which means that the passive stiffness would be measured by stretching the cardiac muscle strip in one direction along a single axis at all times. The axis would be along the orientation that the sarcomeres follow all through the specimen. Such uniaxial tests will under-stress that part of the collagen network that is aligned in the transverse direction with the help of costameres. To explore the transverse contribution of the collagen network, the specimen would have to be subjected to biaxial stress testing wherein there are two axes of loading and unloading, one being perpendicular to another. Biaxial myocardial testing was beyond the scope of our research and we adhered to the uniaxial myocardium test procedure. However, when we interpret our data, from

uniaxial tests, we should recall that the influence of collagen matrix will be marginally underestimated because the specimen is not being biaxially stretched in our experiments.

5.2 The Design Concept
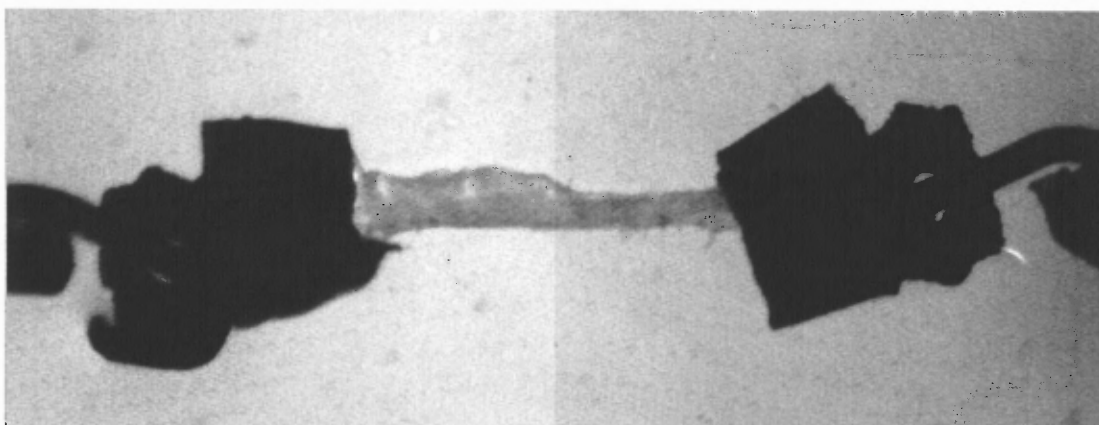
Figure 5.1 Myocardial Strip Mounted for Experimentation.

The objective mentioned in the previous section clearly called for a system that allowed collection of data in vitro on the passive stiffness of myocardium. In the case of the heart there are two types of stress, active and passive. When the heart contracts, intracellular process requiring adenosine triphosphate (ATP) produces active stresses. On the other hand, the myocardium expands during the filling phase of cardiac cycle, and this expansion creates passive elastic stresses. Essentially, stretching of myocytes and the surrounding extra cellular matrix is what accounts for the passive stiffness of heart.

This knowledge implied that the specimen under consideration would have to be stretched experimentally in order to generate passive forces. Therefore a

device was required that would stretch the specimen by an amount that at least simulated the stretch during diastolic filling. This requirement affirmed the need for a stretching device. Since the research was to include contribution to passive stiffness from intracellular fibrils, a device sensitive and accurate enough to stretch a single myocardial cell was initially considered. This would require the device to be capable of stretching the specimen through a few tens of microns.

However, realization of the fact that isolation of a single myocyte for such an experimental purpose was a highly difficult task to achieve, led us to focus on the use of a thin multi-cellular preparation of myocardium instead. The mechanical strain (i.e. percentage-wise stretch) of such a thin strip of myocardium would be set to match the strain expected of sarcomeres as they are stretched over the diastolic range. Hence a stretching device that allowed variable degrees of stretch depending on the initial length of the specimen was required. For a myocardial strip however, much greater range of stretch is required because the initial length of the multi-cellular strip is much longer than a single cell.

Literature suggests that a myocyte cell could undergo a maximum stretch of about 50μm and so a device capable enough to stretch the test cell through this distance was a workable option for this particular method of investigating passive stiffness of myocyte. In case of a thin strip of myocardium put to test, the maximum strain levels would have to be computed with the data available on the sarcomere length at unloaded state and the maximum length a sarcomere could possess. Taking into account the extreme conditions with unloaded sarcomere

length being 1.8µm and the maximum length of the same being 2.4µm, the change in length would be 0.6µm. This would result in an approximate strain level of 33% which is also the maximum strain the sarcomere could achieve without damaging its structure. Now if a myocardial strip, approximately 2.5mm long, was to be subject such strain levels, the maximum change in length that would result in 33% strain would be marginally greater than 0.8mm. Therefore, a device that would offer 0.8mm of stretch to the myocardial strip should suffice for our experimental goals.

Once the device requirement for generation of suitable stretch in passive myocardium was determined, we needed a device that allowed us to compute the stress levels in the specimen. Uniaxial stress can be calculated from measurements of the force exerted in the specimen and its cross-sectional area. Calculation of the cross sectional area is possible just by measuring the specimen's physical dimensions by optical imaging. To measure force values we required a transducer that converts the generated passive forces to a readable electronic data.

It is evident from the literature that the passive stress generated by myocardium can range from less than 1kPa to a maximum of 15kPa. Taking the cross sectional area of the test specimen in its unstressed state as an invariant quantity to calculate stress, which is common practice in muscle mechanics, the maximum stress level would be a result of maximum force being generated by the myocardial strip. A preparation with approximate diameter of 0.25mm would have a cross sectional area marginally less than 0.6mm^2. This implies that a

force of approximately 1mN is sufficient enough to produce a stress level of 15kPa. On similar lines, if active stresses were to be taken into account which reach up to a maximum of 130kPa, the force necessary to generate such a high stress level would be approximately 7.8mN. Hence a force transducer that can measure up to 8mN of force should be sufficient enough to work well for measuring both the active forces and the passive forces generated by the myocardial specimen under examination.

Based on the cross-sectional area of the specimen and the required stress resolution (0.01%), the desired force resolution will be approximately 0.5μN. Assuming equivalent noise levels, a transducer with a working range of ±10mN (capable of measuring both passive and active stress), the minimum signal to noise ratio the device ought to possess is 20,000. Therefore, the transducer with SNR greater than or equal to 20,000, while serving the purpose of measuring passive force, will also effectively reduce the amount of noise that could affect the actual data.

Of course, the force generated would also be dependent on the amount of stretch the specimen would be subjected to. At the same time, a single cell myocyte under test will not generate a force greater than 0.5mN without damaging its structure. In addition, a preparation that had many myocytes would obviously generate greater force, probably up to 1mN, in which case a transducer with lower resolution but greater range would suffice. Owing to the fact that when a stretching device with lower stretching capacity was in place less force would be generated, a force transducer with high sensitivity, resolution and

lower maximum capacity would be a sensible choice. In our case, since a stretching device with high travel range was to be used, it is likely that the transducer with low maximum capacity will not work. Hence, it should be replaced with a transducer having higher range force recording capability. In addition to force measurement, the transducer could also act as the fixed end of the specimen while the other end was being stretched by the translation device.

While generating and recording passive forces, a visualization system was also needed to properly view the muscle strip during the experiment and capture images for extracting relevant data. Since our interests included developing insight at the myocytic level a microscope was definitely needed to view the activity at the sarcomeric level. Since the utilization of this system was more inclined towards functional aspects rather than structural aspects of myocardium, imaging as crisp as that of the electron microscope was not needed. A microscope, sufficient to view the specimen with resolution enough to easily distinguish between two sarcomeres would serve our purpose. An inverted microscope, with objective lens sufficient to resolve sarcomeres, should serve as a feasible option to meet the requirements. Two objective lenses were definitely required to meet our experimental goals. Earlier in this section, it has been mentioned that stress-strain levels would be dependent on the initial length of the specimen and hence we need a reliable technique to compute the same. For this, a complete view of the specimen mounted on the scope was required which could be easily fulfilled with a 1X objective that has 3-4mm field of view. Hence the need of 1Xobjective was affirmed. Furthermore, the sarcomeres were also to

be viewed under the microscope and so an objective was required for the same purpose. Naked eye is capable of visualizing fairly effectively from size 50μm onwards. Considering the sarcomere length at unloaded strain, it would require to be magnified by at least 30 times to have them visible to the eye, of course through the eyepiece. An objective with 40X magnification would increase the ease of visualization of sarcomeres since this objective would visually enhance the length of the unloaded sarcomeres to about 70μm. An objective beyond this level of magnification is not advisable because with increase in magnification power of the lens the working distance reduces and also most objectives beyond 40X objective are oil immersion lenses, which are nowhere compatible with experimental design requirements. And hence a 40X objective was a feasible choice to view the sarcomeres and their orientation throughout the test specimen. In addition, objectives with intermediate level of magnification were required to effectively mount the specimen on to the system for experimentation.

In addition to visualizing the specimen, the inverted microscope also acts as a backbone to support the previously mentioned systems. Using the inverted microscope we can view the complete stretching process. As an add-on to the microscope, a high speed camera would allow capture of digital pictures that would not only serve as a record but would also be instrumental in calculating physical parameters of the specimen with the help the right image processing tool.

Now that we had noted down the requirement of the skeletal structure of our setup, we then had to move on with achieving the functionality of the system.

In other words, we required a control system that would bind the instruments together and allow effective coordination of the entire system. It should also act as an interface between the system and its user while facilitating the ease of operation. Ideally, a good data acquisition system should engulf all these requirements. Hence we realized the need of a strong and efficient data acquisition system.

The following sums up the major requirements of the experimental system under development: a stretching device, a force transducer, an inverted microscope with high speed digital camera and a data acquisition system.

A firm platform was required to support the above mentioned system, so that the setup would be isolated from external vibrations and interference. A regular sturdy table would not serve the purpose, however, as it would not be able to effectively reduce noise signals that would otherwise be combined with the data being acquired. A horizontal surface that could be kinetically controlled with pneumatic balance systems ideally served the purpose of noise reduction, horizontal leveling and vibration isolation of the system.

There were other hurdles to be overcome in order to realize a complete design for the experimental setup. The specimen had to be stretched, could not rest on a glass slide and had to be suspended in the buffer solution. Hence a mechanism was required to connect the test myocardium to the transducer and the stretching device while the specimen was submerged in the relaxing solution.

To provide a means to connect the muscle strip to the force transducer and translation stage and suspend the strip in physiological solutions, fine clips

with minimal surface tension could be attached to the ends of the myocardial sample. These clips could be connected to specially designed hooks extending out of the transducer and the translation stage. To hold the relaxing solution, a chamber was required that would not only be able to house the test specimen during experimentation but would also allow successful imaging required during the experiment. For this, a glass microscope slide was exactly what was needed to form the bottom of the chamber.

For the dissection of heart and preparation of myocardium test specimen, the required instruments were more or less known, owing to the available expertise for the same. Tweezers, scalpels, stereo dissection microscope, gooseneck lamp and other miscellaneous lab supplies were required to serve this purpose and were also readily available.

Now that the design concept was ready, practical realization of the same was next in line. The following chapter discusses the instruments that were picked to realize the system necessary to perform experiments.

CHAPTER 6

EXPERIMENTAL SETUP

6.1 Overview

The research objective, mentioned in the first chapter demanded a sophisticated experimental setup. Figure 6.1 shows the complex experimental setup as it was ultimately assembled to enable us mount the cardiac muscle fibers, stretch the same fiber by a predefined percentage of fiber length and at the same time acquire data about tensile force and sarcomere length.
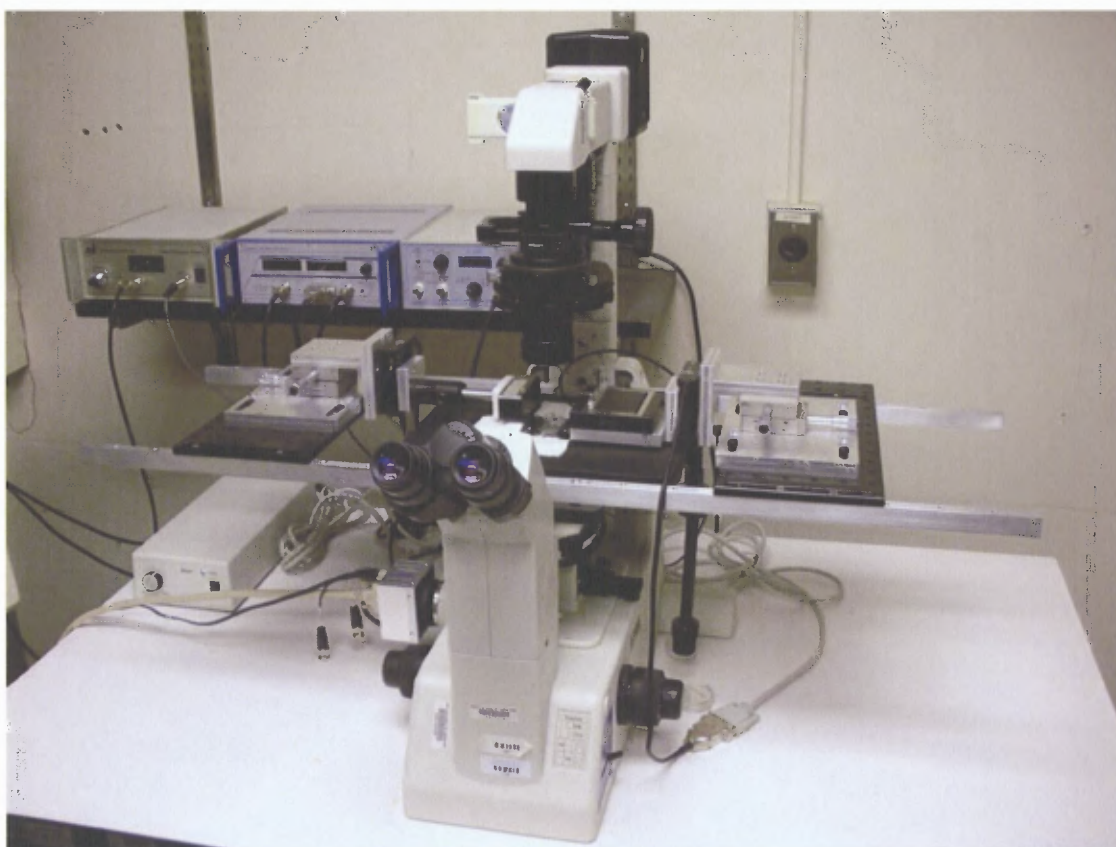
Figure 6.1 Experimental Setup.

A piezoelectric positioning system with 10nm resolution was used to stretch the test specimen through a desired length. The force was measured by a transducer coupled to the end where the fixed part of the cardiac muscle fiber was to be anchored. Additional manual and motorized micron scale positioning stages were used to set the initial length, position, and orientation of the muscle specimen.

As seen in figure 6.1, the inverted microscope, in addition to serving the purpose of microscopy, also stationed the various positioning systems. One optical port on the microscope also housed a CCD camera that allowed live streaming of the stretching process as viewed under the microscope.

This chapter shall document all the equipment and systems that were used for experimentation, while providing a brief knowledge of the same. The technical specifications of the major devices have been included in Appendix A.

6.2 Force Transducer System

From the family of force transducer systems, provided by Aurora Scientific Inc., model 406A with a range of 0.5mN was initially used for our preliminary experiments. This was later to be replaced by model 405A that had a range of 10mN.

The design of these transducers was based on a variable displacement capacitor. Vacuum-deposited metallization on the surface of cantilevered fused silica beams formed the plates of this capacitor. The device had two capacitors, one for active force measurement and the other a reference standard. When a

force is applied the beam bends and the value of the force capacitor changes. The electronic difference between the two capacitance values is proportional to the force applied. The thermal effects and mechanical vibration, as well as pick up of external noise sources such as power line interference, affects both the reference and force measurement capacitors equally. The subtraction process cancels any disturbance that occurs to both devices simultaneously. This is a physical analog of the circuit technique known as common mode rejection and at least 20dB improvement in signal to noise ratio is gained from it.

Figure 6.2 Force Transducer System.
Source: www.aurorascientific.com

Internally, a 1.1MHz sinusoidal oscillator drove both the force measurement and reference capacitors. The transducer head had a detector circuitry that converted high frequency AC to DC signal proportional to the value of each capacitor. The signal then goes to the electronics where a differential transimpedance amplifier converted the current signals to proportional voltages. A differential amplifier generated the difference between these two signals and

the resultant signal passed through a buffering amplifier that also provided controls for offset and amplitude scale factor.

The linearization circuit linearized the signal and the same passed on to the front panel through a gain circuitry. Linearization was required due to the fact that the capacitance change as a function of gap was non-linear. In fact, a different correction function needed to be applied for positive and negative forces since the capacitance varies as a 1/d function, where d is the separation between plates. A piece-wise linear approximation was used. This is done with a 4 diode break-point network which improves the typical 10% full scale non-linearity to better than 1%. Of course, for less than full-scale response, the correction was even better; at 50% of full scale, the typical linearity is 0.2%. Refer Appendix A.1 for device specifications.
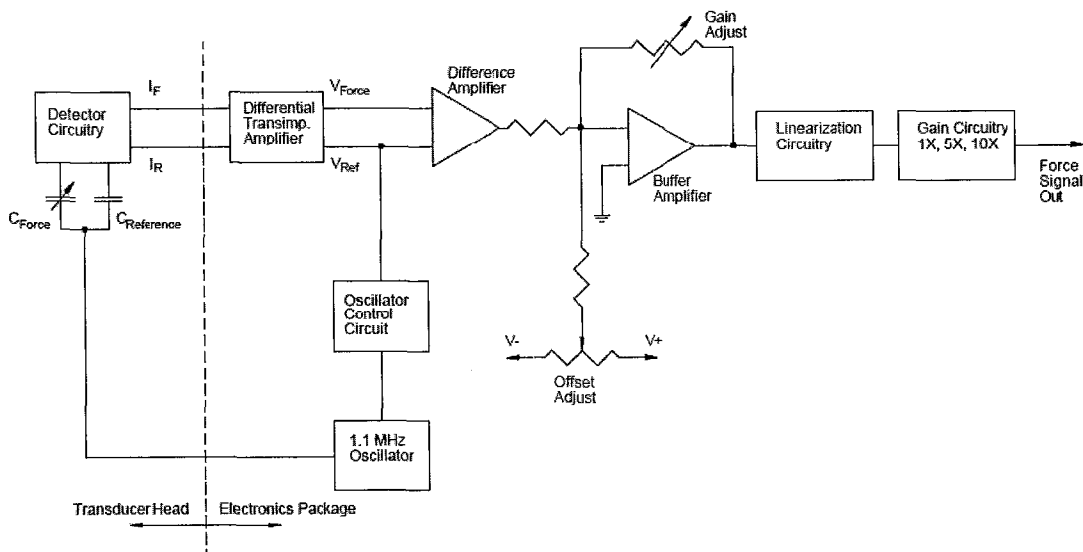
Figure 6.3 Block Diagram of Force Transducer Electronics.
Source: 400A.manual.r7.doc, Aurora Scientific Inc., 2003

6.3 Digital Controller
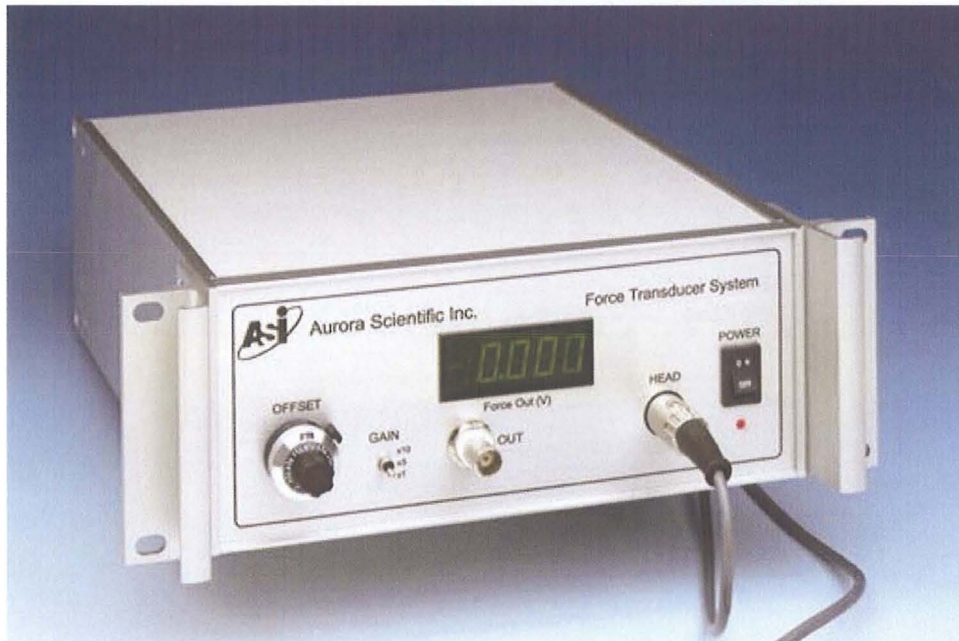
Figure 6.4 Digital Controller for the Force Transducer System.
Source: www.aurorascientific.com

The 600A digital controller was used to study the dynamic mechanical characteristic of muscle tissue. The digital controller system was comprised of custom software for data acquisition, instrument control and data analysis, a small-footprint PC, a data acquisition card and a model 604C Signal Interface (discussed later).

The software had an easy-to-use graphical user interface written using the C programming language. The software collected high-resolution length and force data while controlling the length of the muscle tissue under test. The analog length command signal generated and transmitted via the signal interface (see figure 6.5), served as an input to the piezoelectric translation stage. A distinctive characteristic of the 600A Digital Controller was that the PC used a real-time

operating system (Linux-RT) that ensured time critical data acquisition and control tasks were controlled with a timing accuracy of better than 10µs regardless of other programs and processes that were being run on the computer simultaneously. Refer Appendix A.2 for system configuration and device specifications.

6.4 Signal Interface

Figure 6.5 Signal Interface.

The model 604C signal interface allowed seamless connection of the length controller and force transducer to the A/D system. As seen in figure 6.5, all the connections to the A/D card were made available through the front panel mounted BNC connectors.

6.5 Piezoelectric Linear Stage

The piezoelectric stage used for purpose of stretching the muscle fiber was supplied by Physik Instrumente LP. Initially, when a smaller preparation was contemplated, a piezoelectric stage with a linear travel range of 250µm (P-622.1CD) was used to stretch the myocardial fiber. However, as the chapter

on design criteria explained, when a larger myocardial specimen became the focus for research, this stage failed to offer the necessary percentage of stretch to obtain complete data. Hence it was replaced by another piezoelectric stage that has a linear travel range of 800μm (P-628.1CD). The unit is extremely compact and has rapid response time of 30ms with high accuracy of 10nm. The long travel range is achieved with a friction free and extremely stiff flexure system, while the superior accuracy of unit is due to the direct metrology by capacitive sensors.
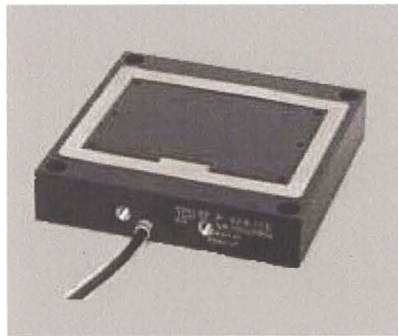
Figure 6.6 PI Hera® Piezo Linear Stage with 800μm linear travel.
Source: www.pi-usa.us

6.6 Piezo Amplifier / Servo Controller

E665.CR LVPZT-Amplifier/Servo bench-top linear amplifier and position servo controller was used to accurately position the piezoelectric linear stage mentioned earlier. The controller has an integrated 20 bit high speed RS232 interface with network capability up to 12 channels.

Figure 6.7 E-665.CR LVPZT – Amplifier / Servo.
Source: www.pi-usa.us

For our purpose, both the RS-232 interface and the analog interface were utilized. The RS-232 interface allowed the transmission of translational data from the piezoelectric device to the data acquisition system via the signal interface. The analog input was used to transmit linear voltage signals, that it received from the signal interface and would in turn direct the motion of the piezoelectric linear stage. The technical specifications for this device can be found in Appendix A.6.

6.7 Micro Translation Stage

In our experimental set up, two micro translation stages (model # M-111.1DG) were used in order to provide one-dimensional vertical adjustment of the force transducer and the piezoelectric linear stage. These translators allowed control of the vertical position of the myocardial specimen in the muscle bath and alignment of the specimen axis parallel with the horizontal axis. These ultra high resolution

motorized translation stages provide linear motion of 15mm. Each stage is equipped with a lead screw for precise motion with reduced friction. The stage is driven by DC motor gear head.
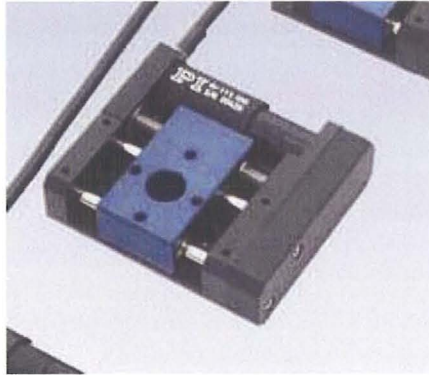
Figure 6.8 Translation Stage M111.1DG.
Source: www.pi-usa.us

The translation stage seen in figure 5.8 is controlled by DC motor controller which receives commands from the 2-axis handling utility provided by Physik Instrumente LP. Motorized control was required for more accurate and precise alignment and co-ordination between the two stages.

6.7.1 DC Motor Controller

The Mercury II palm top DC motor controller, model number C 862, is a low cost high performance solution for position control of the translation stage. The use of two mirco translation stages demanded two DC motor controllers in order to exercise individual control over each stage.
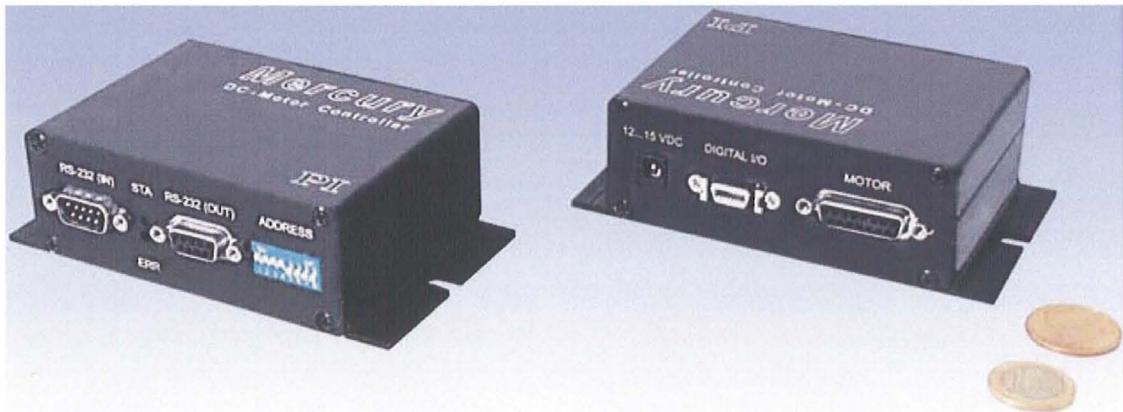
Figure 6.9 Front and back view of Mercury II DC Motor Controller.
Source: www.pi-usa.us

These motors have an in-built amplifier and possess stand alone functionality. The controller's highly specialized processor provides high performance PID motion control with required trajectory generation and filter settings.

6.7.2 Handling Utility

The Mercury joystick 2-axis handling utility for C-862 Mercury controllers, a software and hardware package, was used to provide direction and commands to the DC motor controllers which in turn positioned the micro translation stages. A dedicated computer was used to support this system.

With the help of a joystick the two motorized stages were translated in the vertical direction either one at a time or both simultaneously. As seen in figure 6.10, only the encircled button was used to control the two stages. If the button was pushed up or down just the translation stage connected at the force transducer end would either lower or rise respectively. And the other translation stage would raise or lower the piezoelectric stage if the same button was pushed

left or right respectively. Simultaneous motion of both the stages was made possible by pushing the same button at 45^0, 135^0, 225^0 or 315^0 depending on the required combination of motion. For instance, pushing the button at 45^0 would lower both the stages at the same time and pushing it at 225^0 would raise both the stages together.

Figure 6.10 Joystick for Translation of Motorized Stages. Only the encircled button is to be used to control the motion of both the stages.

6.8 Linear Slide

While the previous devices controlled the vertical position of the myocardial specimen in the muscle bath, the horizontal X-Y position and orientation of the specimen was controlled by two sets of manual slides. These positioned the force transducer and piezoelectric translation stage in the X-Y plane. These

manual adjustments were used to set the initial length of the myocardial fiber. They were also used to position the specimen over the optical axis of the microscope so that a region of the fiber with clearly evident sarcomere pattern was visible.

Four manual linear slides, with a travel range of 15mm each, were used to position the force transducer and the piezo stage in the XY plane. The M-011.00 stage is equipped with a high precision manual micrometer facilitating a sensitivity of 1µm.

In order to achieve motion in the XY direction, two stages are coupled together at both the ends. In effect, 15mm ultra straight motion is achieved in both X and Y directions. Figure 6.11 illustrates XY combination of the stages.
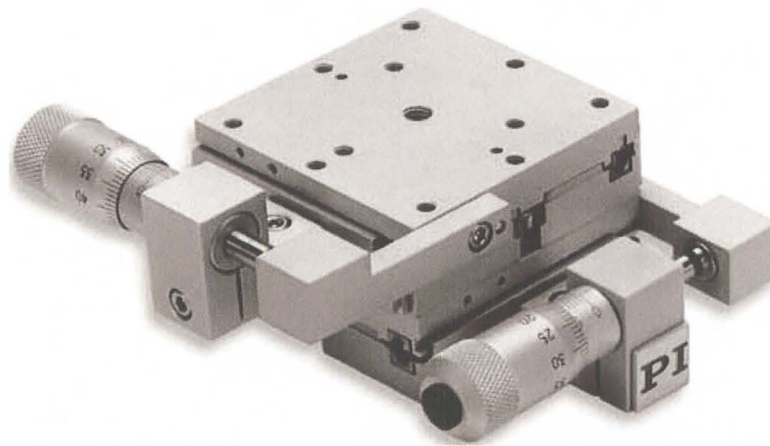
Figure 6.11 XY Combination of Two Stages.
Source: www.pi-usa.us

6.9 The Inverted Microscope

6.9.1 Nikon Eclipse TE 200 Inverted Microscope

The inverted microscope is the backbone of the experimental setup and provides base for the transducer measurement systems. It also has a digital camera (Imperx) attached to it that allows us to capture pictures on the test specimen. The microscope also houses 4 objectives, each with a different magnification power.

Figure 6.12 Nikon Eclipse TE 200 Inverted Microscope.
Source: www.nikoninstruments.com

6.9.2 Objective Lens

The following four objectives were used to view the specimen at a variety of magnifications:

1. Nikon Plan UW 1X / NA 0.04 WD 3.2

2. Nikon LU Plan 5X / NA 0.15 EPI

3. Nikon 10X / NA 0.25 WD 6.1

4. Nikon Plan Fluor ELWD 40X / NA 0.60 WD 3.6-2.8

The abbreviated objective designations are as follows:

UW – Ultra wide

NA – Numerical Aperture

WD – Working Distance (in mm)

LU – Nikon Luminous Universal

EPI – Oblique illumination

ELWD – Extra Long Working Distance

Plan – Apochromatic and Flat Field correction

Fluor – Fluorite aberration correction

Figure 6.13 Objective Lens with 1X, 5X, 10X, 40X Magnification, left to right.
Source: www.nikon instruments.com

6.10 CCD Camera

Figure 6.14 Imperx CCD Camera (IPX-VGA210-L).
Source: www.imperx.com

The Imperx camera shown in the figure 6.14 was utilized, without its lens, to capture the entire protocol execution under the microscope as well as capture images of the specimen, mainly under 1X and 40X magnification, for further analysis. The default camera lens was discarded as the image that was being projected on the camera had already passed through a system of lenses.

The IPX-VGA210L is a monochrome high-speed progressive scan, fully programmable CCD camera with a resolution of 640X480. It has a high frame capture rate of 210 frames per second, Camera Link (CamLink) output which is a serial communication protocol designed for computer vision applications, and powerful features and flexibility that give high quality images. For technical specifications please refer Appendix A.8.

6.11 High-speed Video Sarcomere Length System

The 901A High-speed Video Sarcomere Length (HVSL) system provided by Aurora Scientific Inc. was used to capture images that were sent out by the Imperx CCD Camera. The system has the capacity to capture images and calculate sarcomere length at an even higher rate frame rate than the CCD camera. Though we did not use HVSL system to calculate sarcomere length, it gave us images which were then loaded on Image J to compute the initial length of the preparation and the sarcomere length.

The system comprises of HVSL software, a control PC and a camera interface. The HVSL software and hardware operates on a dedicated linux PC. The HVSL was used to view the protocol execution and to store images of the specimen required for further data processing.

6.12 Vibraplane

The Kinetic Systems Vibraplane was used to provide a vibration free environment for the complete experimental setup. This primarily helps to protect the microscope from sudden mechanical shocks and also serves to reduce noise from mechanical vibrations during experimentation. The plane isolates sensitive instruments and experiments from the surrounding vibrations. Apart from vertical and horizontal vibration isolation the vibraplane maintains a preset zero deflection level regardless of load addition or removal. The isolation workstation has 70% vertical vibration isolation efficiency at a natural frequency of 5Hz and 64% in the horizontal direction.

Figure 6.15 Kinetic Systems Vibraplane.
Source: www.kineticsystems.com

6.13 Automatic Temperature Controller

The temperature of the physiological solution in the muscle bath was maintained by the single channel heater controller. This thermal control device from Warner Instruments Inc. was utilized in automatic mode to provide total automated control of the bath temperature at a preset value.

Figure 6.16 Single Channel Heater Controller (TC-324B).
Source: www.warneronline.com

The device was fundamentally comprised of two thermistor, one functioned as temperature sensor and the other as self-regulating heating elements. Two 3-pin connectors, which served as input-output channel to the controller were plugged into the conductive ports available at the sides of the bath slide (see figure 6.19).

Once the temperature controller was fed with a control temperature value and the automatic mode turned on, the controller would automatically turn on and off the supply of heat depending on the temperature of the chamber and thus maintain the temperature levels of the physiological solutions in the chamber.

6.14 Stereo Dissection Microscope

In order to prepare specimens from heart tissue, a basic stereo dissection microscope was used. This microscope from Fisher Scientific had 10X and 20X magnification. This magnification was achieved by the use of a 10X eyepiece with 1X and 2X objectives.

Figure 6.17 Fisher Scientific Stereomaster Microscope.
Source: www.fishersci.com

6.15 Miscellaneous

Apart from all the devices and instruments mentioned so far in this chapter some other essential tools and materials were used to complete the experimental setup. Machined aluminum metal was used to firmly support the transducers and the translation stages. A light source (Schott ACE) was used with a goose neck fiber-optic light source guide to provide well controlled lighting light while preparing test specimens under the stereo dissection microscope.

Metal hooks extended out of the force transducer stage and the piezo translation stage to enable mounting the test specimen, end of which were attached to metal T-clips.
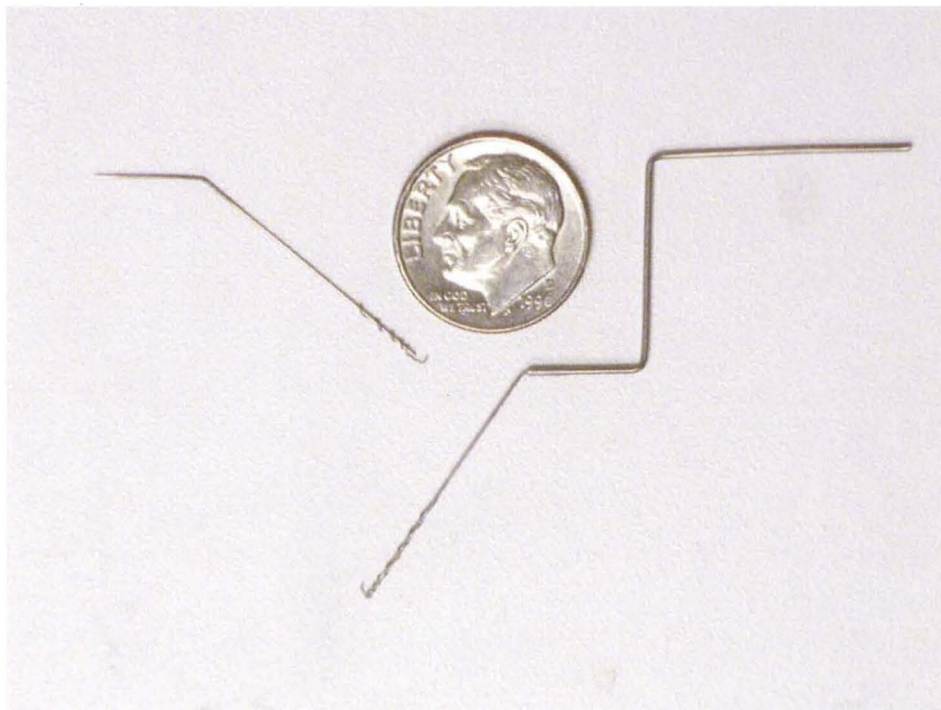
Figure 6.18 The Metal Hooks; with a Dime for size comparison. The hook on the left extended out of the force transducer, while the other was mounted on the piezoelectric translation stage.

The bath slide held various physiological solutions in which the specimen was suspended while under observation. The solutions are carefully exchanged with the use of pipettes, while minimally disturbing the specimen.
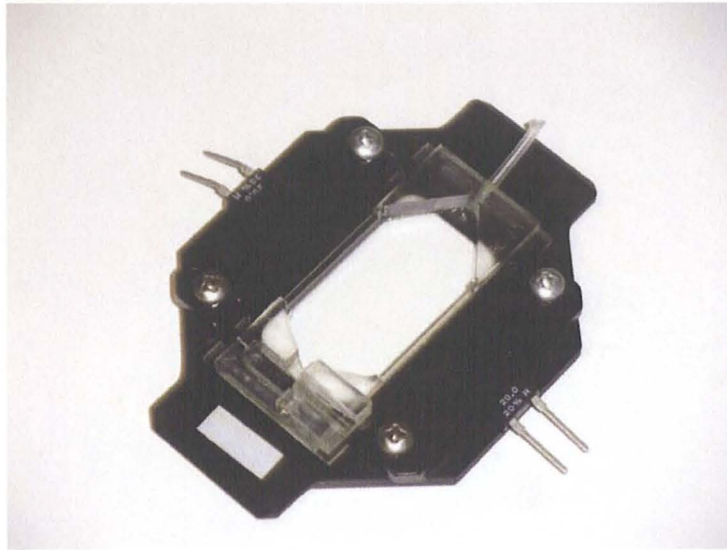
Figure 6.19 Bath Slide.

Other apparatus like forceps, scalpels, tweezers and transfer pipettes were used to carefully prepare and handle the test specimen. In addition to these instruments, a variety of physiological solutions were used to maintain the myocardium in a passive, fully-relaxed state before and during the experiment. The next chapter shall discuss more about the physiological solutions used and their role in the trials.

CHAPTER 7

EXPERIMENTAL PROCEDURE

The entire experimental process was composed of various different phases viz. preparation of specimen, mounting the same on the stretching system, performing tests to determine passive stiffness, capturing images, acquiring data so on and so forth. This chapter intends to describe all the stages that make up the entire experimental procedure developed.

7.1 Specimen Preparation

The process of specimen preparation has been adopted from similar cardiovascular research that is underway at Washington State University, Pullman, Washington. Dr. J. P. Marquez underwent a training program at WSU and then transferred the knowledge and expertise to us in order to carry on with the research.

Prior to dissecting the heart, the buffer solution was prepared. This solution, also known as relaxing solution, was used to preserve the integrity of the tissue while in frozen state and it also produce an environment in which the tissue could be guaranteed to be in a relaxed state. A relaxed state implies that there are no myosin cross-bridges attached to actin. Two components of the relaxing solution ensure a relaxed state: 1) Butanedione Monoxime (BDM) blocks the myosin cross-bridges from binding with actin, and 2) EDTA (a Ca^{2+} chelator) to keep the concentration of free Ca^{2+} ions below 0.1µM so that the troponin will

not be activated by Ca^{2+}. Apart from the buffer solution, two depolymerization solutions were also used to depolymerize the thick and thin filaments (and so remove titin's anchor point) during the trial that in effect allowed us to find the contribution of collagen alone to the passive stiffness of heart. For details on the composition of these solutions, refer to Appendix C.

The hearts that were used in our trials mainly came from transgenic rats or pigs otherwise. The heart, if frozen at $-80^{0}C$, was kept in relaxing solution at -20C for 2 days. In some preliminary experiments the animal was sacrificed on the day before the experiment and so fresh unfrozen tissue was used immediately.

From the heart, specimen of length 2.5 – 3mm and approximately 0.2mm wide were carefully cut out while the heart itself was held in a dish filled with relaxing solution. The fibers were cut out in directions parallel to the epicardial fiber direction (parallel to small blood vessels) and achieved a uniform and parallel orientation of sarcomeres.

While the fibers were being cut, T-clips were immersed in alcohol to eliminate the surface tension. A T-clip was then attached to each end of the cut fibers. These fibers, with the T-clips attached, were then "skinned" overnight in relaxing solution with a detergent (1% triton X100). The skinning process gets rid of the cell membrane and the membranes of the cell organelles that control the flow of ions and molecules in and out of the cell or organelles. This was done to ensure that any free Ca2+ present would not be able to activate the cell and thereby enabling us to exercise complete control over the activity of the test fiber.

7.2 From Mounting to Pre-conditioning Precursor

A skinned fiber was then picked up and carefully mounted on the system that performs the stretching process while the specimen was fully submerged in the relaxing solution contained within the muscle bath. The specimen fiber was mounted with the help of T-clips onto the hooks that extended out from the force transducer and the piezo translation stage on either side.

The specimen was then positioned with the help of manual translation stages in such a manner that there would be no slacking of the fiber and the T-clips would be aligned in a horizontal line. This particular process required skills so as to set the initial specimen length, for each experiment, such that the compliant region of response to passive stretch would be completely captured during the experiment. For this, first the slack of the mounted fiber would be removed with the help of manual translation stages at both the fixed end and the piezoelectric translation stage end. The adjustment of the clips on the hooks is checked so that during the stretching process the hooks and the clips behave as a single unit such that there was no motion in between them. The specimen is then just stretched enough so that we would not lose the data pertaining to the complaint response of the specimen. This procedure required practice to ensure reproducibility, which was well substantiated by the preliminary results.

At this juncture, images under 1X objective were captured. These images were immediately processed using the software Image J in order to determine the length of the specimen that was visible between the clips and would actually participate in force generation during the stretching process. The same images

were also used to determine the average diameter of the preparation. Further details on the image processing technique will be discussed towards the end of this chapter. The unstressed length of specimen was computed, and the value was used to determine the distance through which the specimen was to be stretched to achieve the desired strain.

With the P-628.1CD piezoelectric translation stage, which had a capacity to travel up to 800µm, test for effective mounting of the specimen could be done easily. For this, the specimen was subjected to a 200 - 300µm stretch for up to 5 times to check whether or not the specimen was responding well to the test and also to ensure proper mounting of the tissue. This procedure served as a precursor to pre-conditioning process that followed.

Also, all through during the entire experimental procedure the temperature of the muscle chamber was maintained at 25^0C using a temperature controller.

7.3 The Passive Force Generation and Data Acquisition

Upon successful completion of mounting process, a sequence of stretch protocols was created using the sequencer tool available with the software system for data acquisition. The test protocol was selected on the basis of the specimen length value obtained from its image taken under 1X objective. Protocols for various stretch levels were written to accommodate a larger pool of different specimen lengths. Refer Appendix B for stretch protocols.

The stretch sequence also incorporated the pre-conditioning process to ensure that the specimen gets well acquainted to the subjected strain levels. The

initial protocols of the sequence were aimed exactly ensuring proper response of the specimen to the test.

The stretch sequence was designed to pull and retract the fiber at least 10 times while acquiring the data simultaneously and saving it at the desired location. This acquired data gave us the change in length of specimen and the force it generated during the process.

7.4 Image Capture for Sarcomere Length Computation

After the sequence was completed and the data recorded, images of the specimen were captured under 40X objective, wherein the sarcomere pattern would be visible. These images upon further analysis gave the length of the sarcomeres present in the fiber at rest state.

Separate codes were written to stretch the fiber and hold it in the stretched position for a specified amount of time, during which image captured under 40X objective were acquired. These images allowed us to compute the sarcomere length at a stretched state.

7.5 Depolymerization

Now the relaxing solution from the bath slide was carefully replaced by KCl depolymerizing solution, with the specimen submerged in it and kept for 30 minutes. This solution was then replaced by KI depolymerizing solution and the same was kept for another 30 minutes. This treatment was done in order to

depolymerize the thick filaments, remove one of titin's mechanical anchors, and thus eliminate its influence on the passive stiffness of the fiber.

Upon 30 minutes of treatment with KI depolymerizing solution, it was replaced with relaxing solution again and the entire process from pre-conditioning through the stretching sequence with same protocols till data acquisition was conducted again to acquire force and length related data. However, this time only the effect of collagen on the passive stiffness should be visible in the data obtained.

7.6 Image Processing and Data Analysis

The images of the specimen that were captured during the experimentation were then loaded on Image J, an image-processing software suite provided by the National Institutes of Health. The required data was computed using the tools provided by this software. Depending on the *magnification factor of the objective* lens the scale parameters were set, which then enabled the software to report length values in micrometers rather than number of pixels.

Plots for the force and displacement with respect to time were generated using the data that was acquired during the sequential stretching process. Each protocol in a sequence created a new set of data points. The plots from the first stretching sequence reported the combined effect of titin and collagen on the passive force generated by the fiber when stretched. The plots generated from the data acquired after the process of depolymerization reported the contribution of collagen only to the passive stiffness of the fiber.

CHAPTER 8

PRELIMINARY RESULTS

8.1 Measurement of Initial Specimen Length and Average Diameter
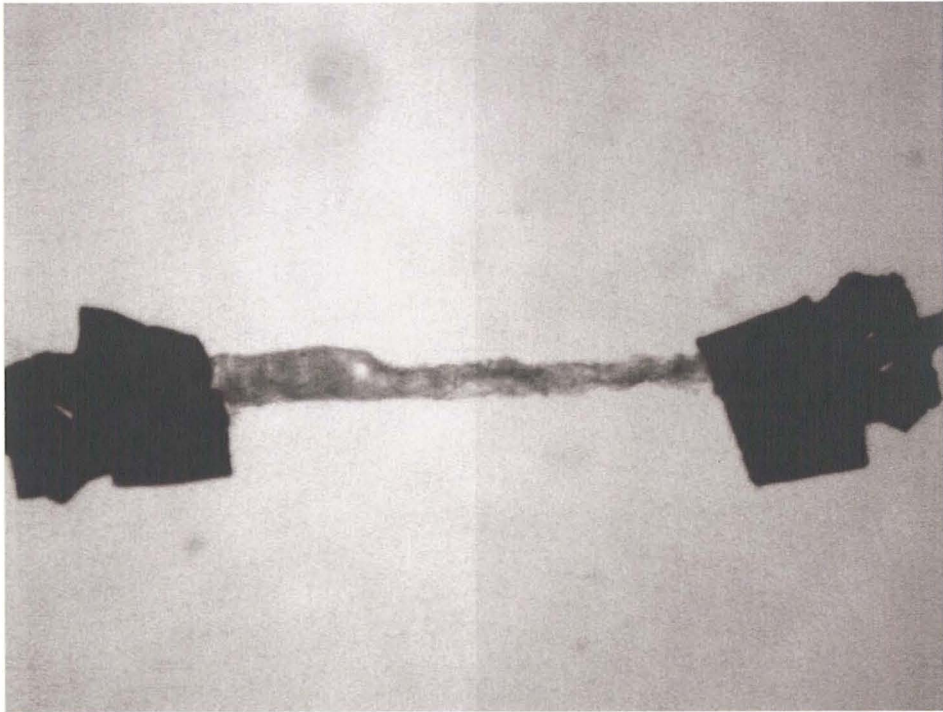
Figure 8.1 Specimen under 1X Objective.

8.1.1 Measurement of Initial Specimen Length

The initial length of the specimen was calculated using the images captured under 1X objective lens. Figure 8.1 shows a typical view from the 1X objective. Images of this type were then loaded on Image J, the Java-based image processing program developed at the National Institute of Health, and the necessary processing then done to obtain the length of the specimen. Figure 8.2 shows a line segment pulled through the length of the specimen, the measure of which would give the length of the specimen.
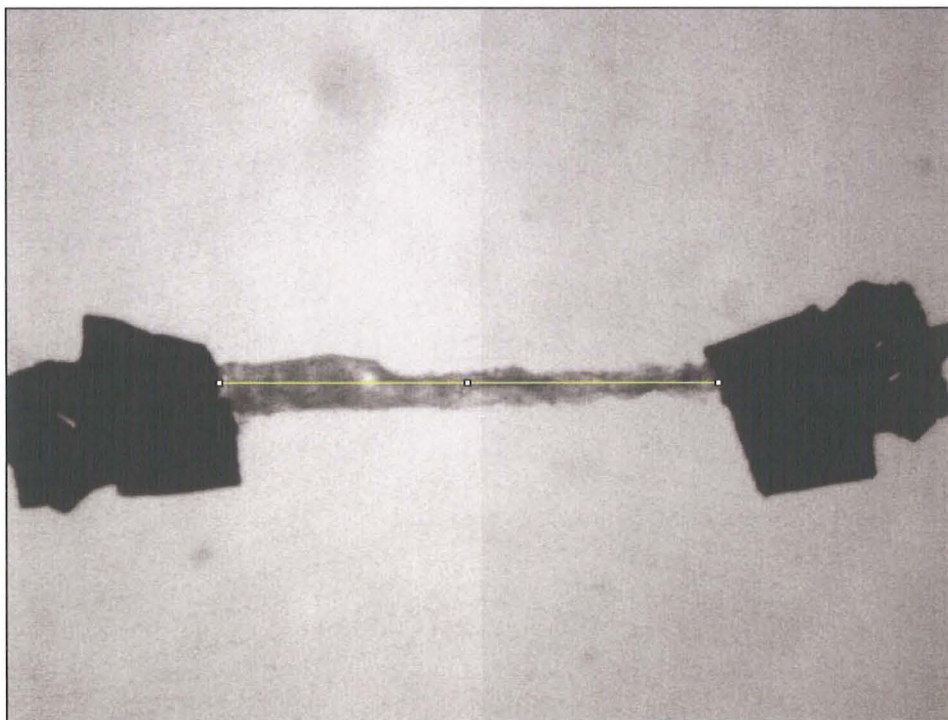
Figure 8.2 Image being Processed Using 'Image J'. Length of the line segment would give the length of the specimen, owing to the right scale factor.

The scale parameters were set according to the magnification factor to obtain results in microns (see appendix D for user-defined scale parameters). Figure 8.3 displays a typical results table generated by Image J. From the results table we can say that the length of specimen was approximately 2.4mm.

Figure 8.3 Results Table; displaying the length of the specimen.

8.1.2 Measurement of Average Diameter

Assuming the preparation to be circular in shape, average diameter of the specimen was calculated using a technique similar to that of initial length measurement. Here the width of the specimen was measured at different location on the specimen using the same image from 1X objective lens (see figure 8.4) and then the average of these would be the average diameter. This value enables us to compute the cross sectional area of the specimen.
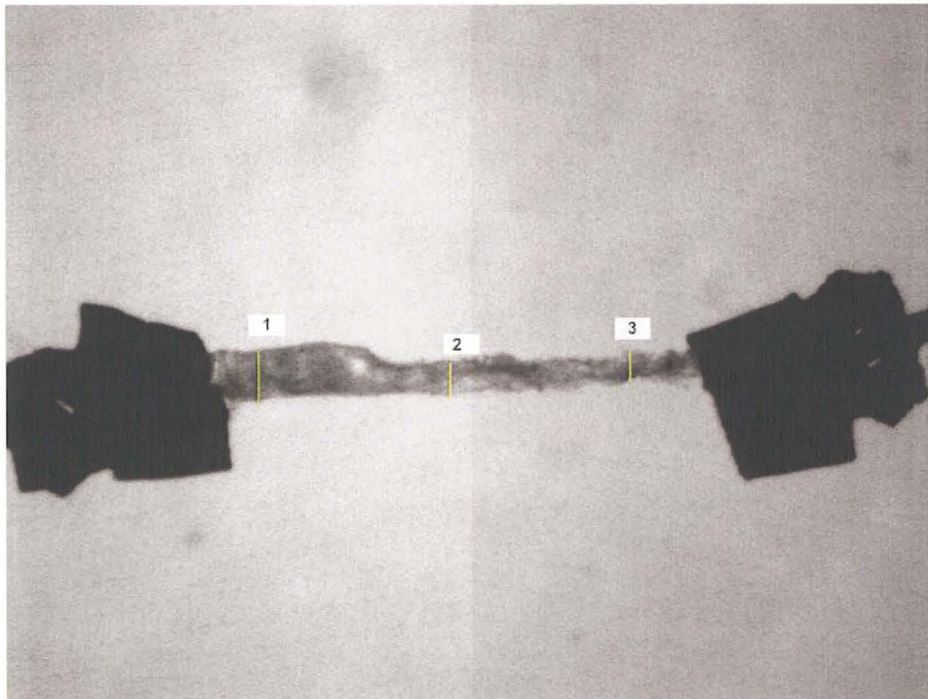
Figure 8.4 Measurement of Average Diameter.

Note that figure 8.4 is not a screen capture from Image J. This image has been created for illustration purposes only. The diameter values at the three different locations were 231µm (at point 1), 150µm (at point 2) and 135µm (at

point 3). The average of these values would result in an average diameter of 0.17mm.

8.2 Measurement of Sarcomere Length at the Initial Specimen Length

As stated earlier, the 40X objective used to visualize the sarcomeres present in the myocardium strip under test. In addition to just viewing the sacromere, the images resulting from the 40X objective also displays the orientation of sarcomere along the length of the specimen. Figure 8.4 shows various images of sarcomere patterns from different specimens.
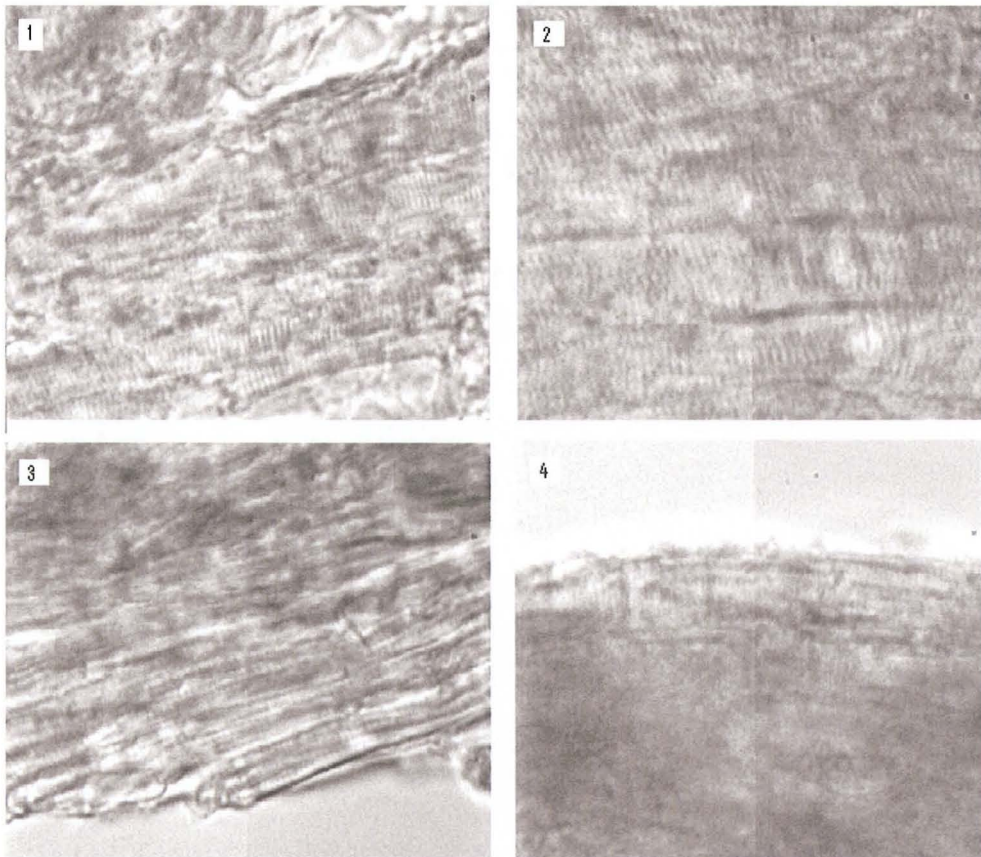
Figure 8.5 Sarcomere Patterns from Different Specimens.

In figure 8.5, image 1 and 2 show sacomere patterns to be in the direction of the preparation. Though image 2 has more visible sarcomeres than image 1, the orientation of sarcomeres in both the cases seemed to be similar. Image 3 shows sarcomeres, at the edge of the cardiac muscle fiber, which were slightly deflected in orientation from an axis parallel to the specimen. Image 4 of the same figure was indicative of both a thick preparation and user inefficiency to capture the right image.

For computation of sarcomere length, images with fairly good visibility of sarcomere pattern were opened with Image J and the length of sarcomere calculated. Here, the total length of a series of sarcomeres (the series has a known number of sarcomeres) was measured and the average of this value was the length of each sarcomere.
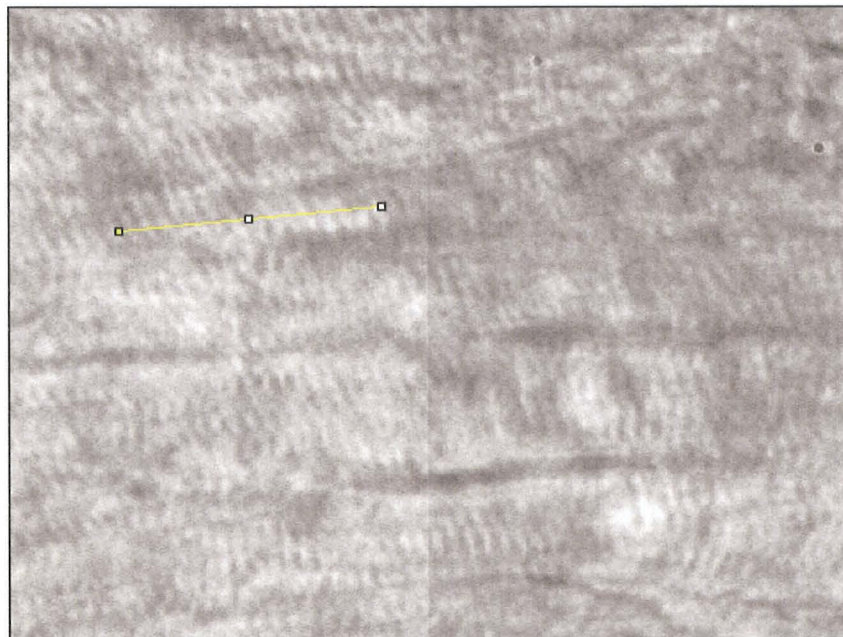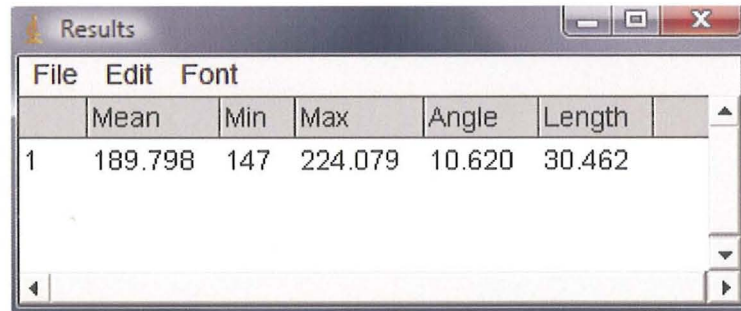
Figure 8.6 Total Length of a Series of 16 Sarcomeres being Measured.

Figure 8.7 Result Table for Measurement of Sarcomere Length.

From figure 8.7, it is clear that the total length of 16 sarcomeres under consideration was 30.462µm, which means the average length of each sarcomere is about 1.90µm.
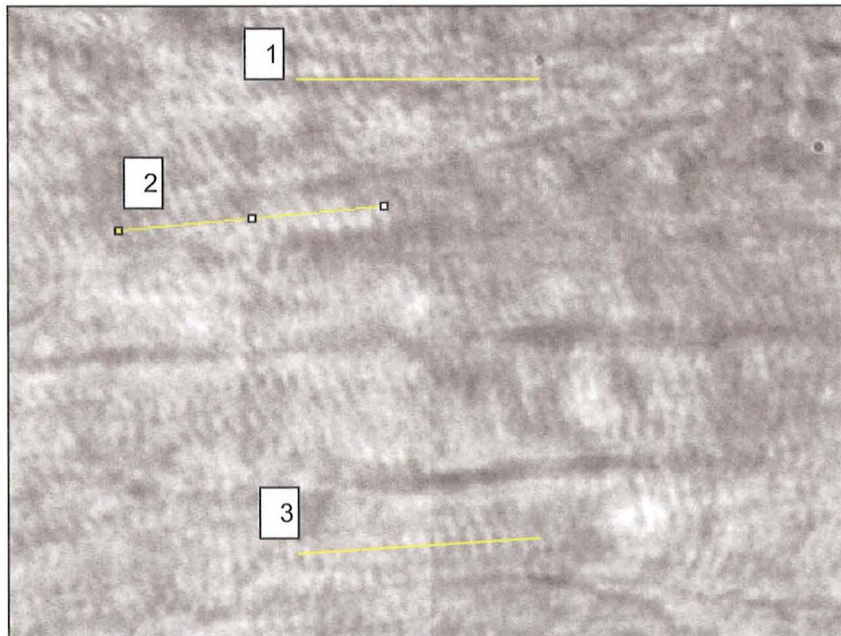
Figure 8.8 Sarcomere Length Measurements.

On similar lines, average sarcomere length was computed at different locations of visible sarcomere pattern with a different number of sarcomeres in

series taken into account (see figure 8.8). The average these of values gave a better approximation of the sarcomere length.

The average sarcomere length at location 1 (21 sarcomeres) was 1.91µm and at location 3 (18 sarcomeres) was 1.88µm. The location 2 is same as previous. The average of these three sarcomere length values is 1.89µm.

8.3 The Stress-Strain Results

To explain the stress-strain results, obtained after subjecting the test specimen to controlled mechanical strain, let us pick a typical example:

Animal : Rat

Tissue : Myocardium

Initial specimen length : 2.6mm

Initial Cross-sectional area : $0.042mm^2$

Initial Sarcomere length : 1.86µm

Subjected strain : 23% (600µm)

Sampling frequency : 10KHz

8.3.1 Contribution of both Titin and Collagen

As mentioned in the experimental procedure, the specimen was first subjected to controlled passive strain to investigate the contribution of both titin and collagen to the myocardial stiffness. Figure 8.9 shows the change in length of specimen over time followed by figure 8.10 that displays the force levels generated by the

specimen while being stretched over a distance of 0.6mm and return back to the initial length.

The graphs in figure 8.9 and 8.10 have not been recorded from the first cycle of stretch and release. It was the data from the 6th cycle that was used to plot the graphs. This was done so as to allow pre-conditioning of the specimen and to get it acquainted to the stretch and release process. Also the sequence used to perform this experiment had incorporated a two seconds delay between the end of one cycle and start of the next cycle.

The data pertaining to change in length was not the value of command signal given to the translation stage rather it was the actual length of tranlsation that is reported back by the device while responding to the command signal.

Figure 8.9 substantiates the efficiency of the piezoelectric translation stage to translate through a specified distance in a nearly linear fashion, i.e. at a nearly constant rate, with the increament or decreament in the control voltage, over a given interval of time. The response of piezoelectric translation stage was near linear and not completely linear due to the inherent losses in the internal circuitry of the device.

Figure 8.10 depicts that the passive force generated by the specimen peaked at a value slightly greater than 0.4mN. The slight irregularity seen during the initial 2-3 seconds of the test is indicative of some clip motion. In a poorly mounted preparation substantial sudden jumps in recorded force occur.
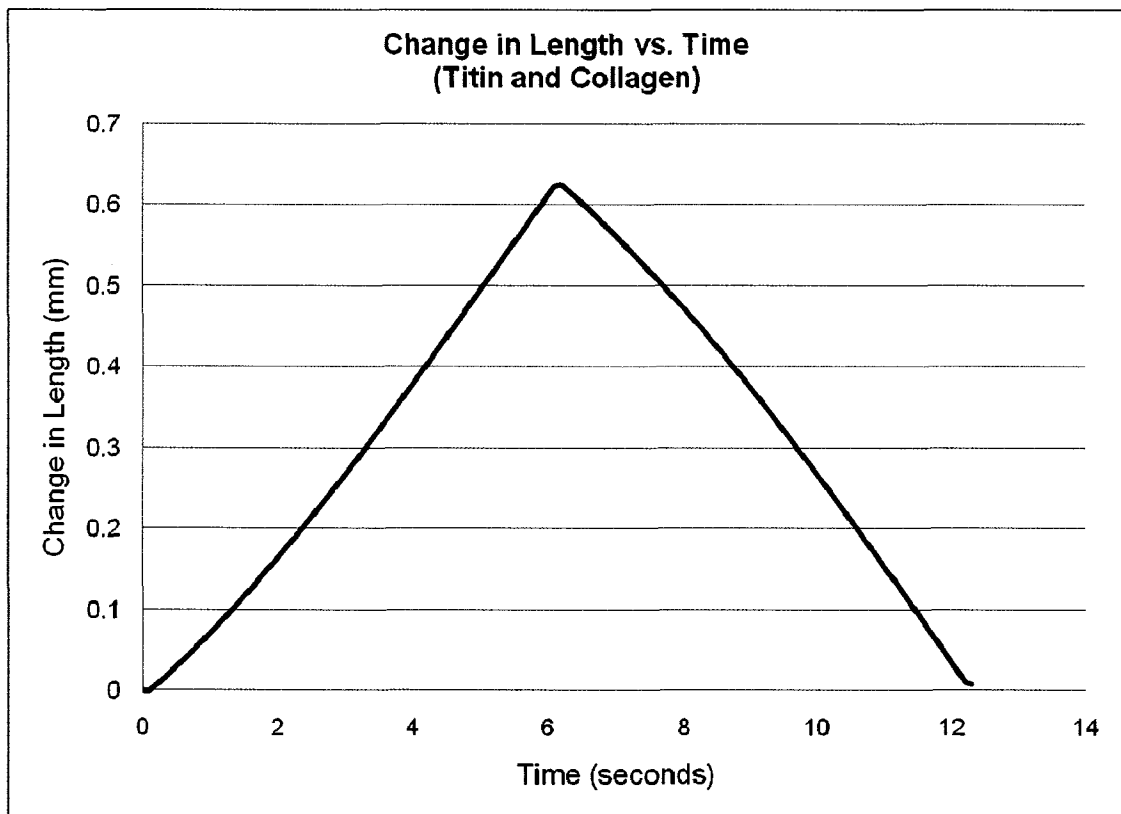
Figure 8.9 Change in Length vs. Time; in Presence of both Titin and Collagen.
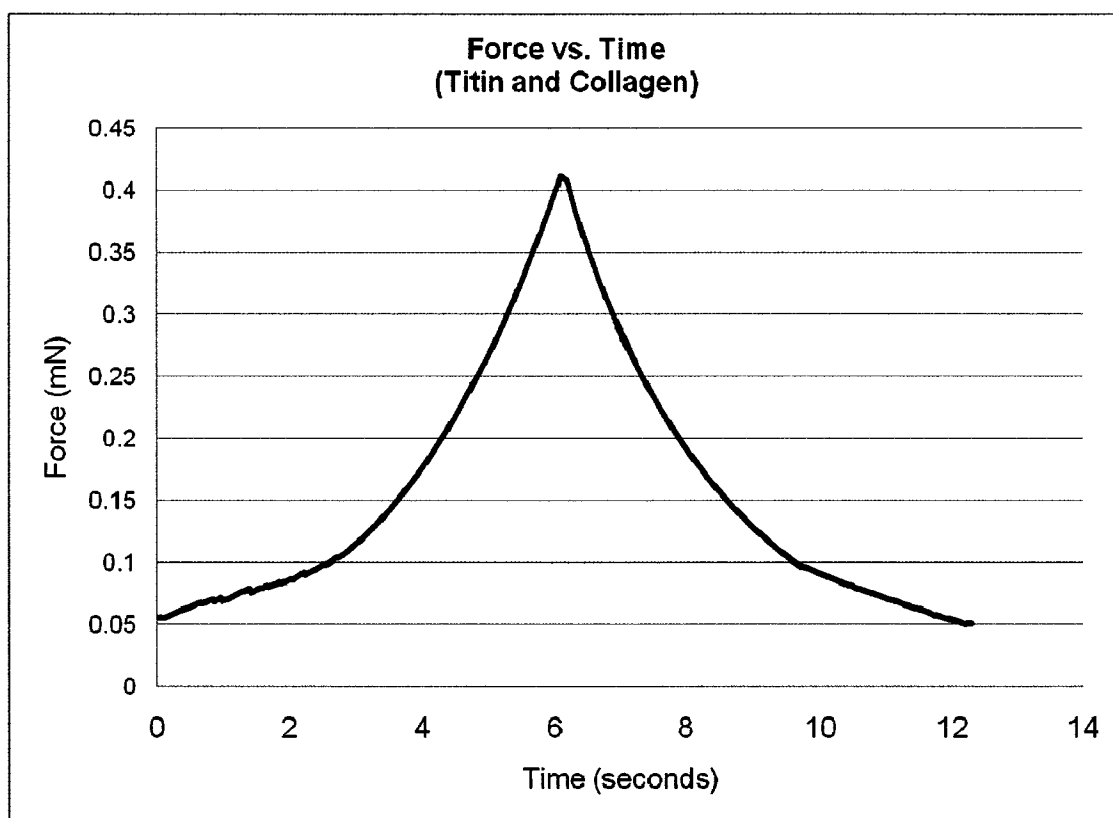
Figure 8.10 Force vs. Time; in Presence of both Titin and Collagen.
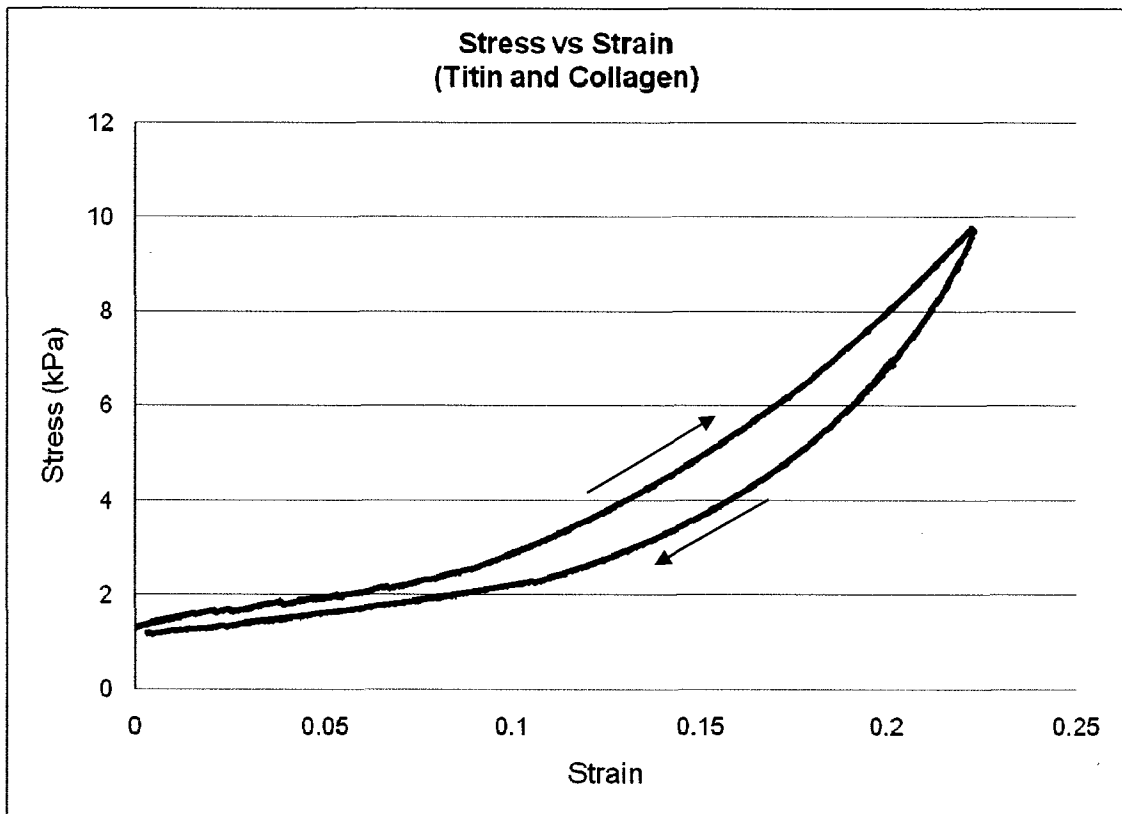
Figure 8.11 Stress – Strain Relationship; in Presence of both Titin and Collagen.

From the available data, we then computed the stress and strain values and the results are very well depicted by the stress-strain graph in figure 8.11.

The concave up shape of the graph in figure 8.11 was indicative of the fact that just like all biomaterials, our myocardial specimen also stiffens when subjected to increased stretched levels. The direction of the hyteresis loop affirms that the specimen was under passive tension dissipating energy in the form of heat. Since the muscle was passive , there was no active generation of energy in form of ATP, thereby, only dissipation of energy in the form of heat due to viscoelasticity occurred. The graph also substantiates the stress levels mentioned in the literature as they match the stress levels generated the by the cardiac muscle strip under test. Also, assuming homogenity, the maximum strain of 23% should be stretching the sarcomeres with initial length of 1.86μm to upto 2.3μm. In reality, the assumption of homogenity doesnot hold true and the average stretch of healthy sarcomere was somewhat less because of more compliant but damaged ends of the preparation.

8.3.2 Contribution of Collagen only

The depolymerization process was the next step in the investigative procedure. This was done by subjecting the specimen to the two depolymerizing solutions – and thus removing titin as a contributor to passive tension – we could thus determine the contribution of collagen alone to the passive force generated by the myocardial strip. During this protocol, the strip was subjected to the same time course of strain as mentioned in the previous section.
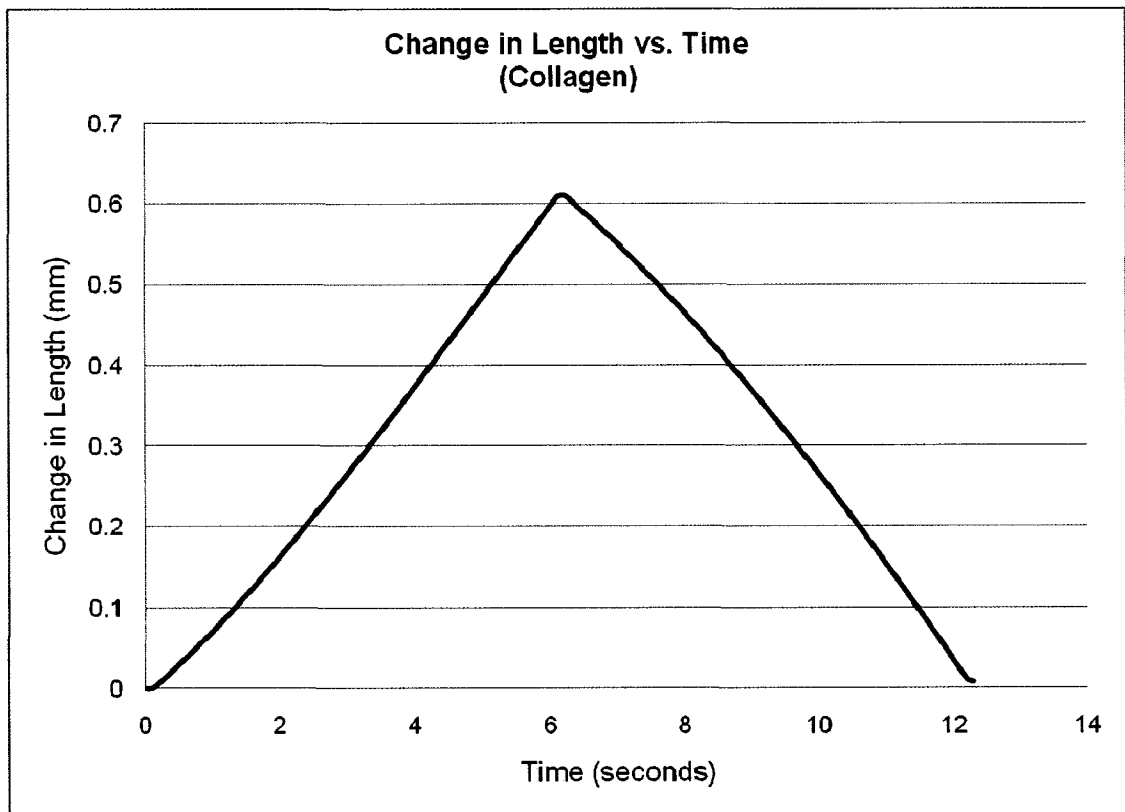
Figure 8.12 Change in Length vs. Time; Presence of Collagen only.
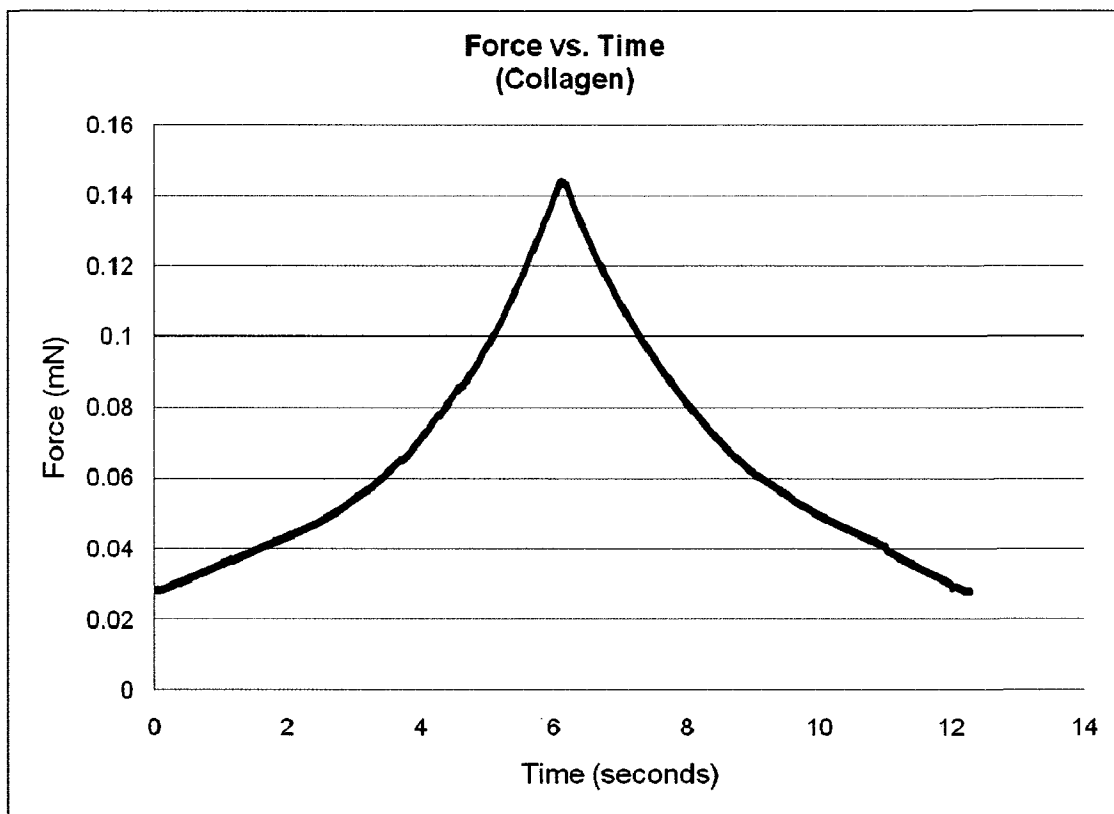
Figure 8.13 Force vs. Time; Contribution of Collagen only.
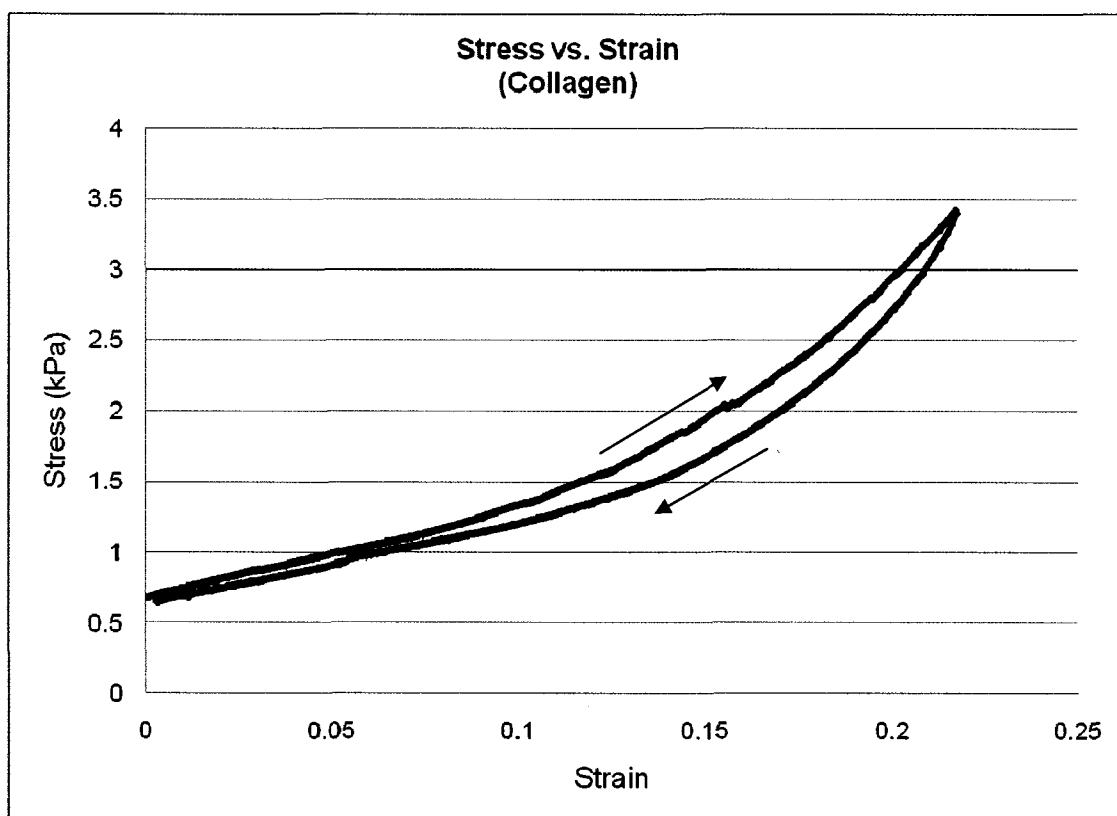
Figure 8.14 Stress – Strain Relationship; Contribution of Collagen only.

The geometry of the graph in figure in figure 8.14 is in accordance with the behaoviour of any other biomaterial when subjected to tension. Also, the direction of hysteresis loop indicates the energy loss in the form of heat. It should be noted here that the stress-strain curve for the contribution of collagen only displays less hysteresis and energy dissipation when compared to the same in case where both titin and collagen were present. Moreover, a reduction of stress levels for the same level of strain can be observed when only collagen contributed to the passive stiffness of the muscle strip.

8.3.3 Contribution of Titin only

The stress – strain relationship for the specimen, owing to the contribution of titin only, was calculated by finding the differnce between the stress-strain relatioships presented in the previous two sections. The resultant is represented graphically in figure 8.15.

In order to determine the accurate corresponding strain levels, difference between the strain values, used to plot curves in the previous two section, recorded at the same time interval, was computed. The resultant of this turned out to be close to zero and hence the strain values used to plot the stress-strain curve for the contribution of both titin and collagen were re-utilized to plot the graph in figure 8.15.
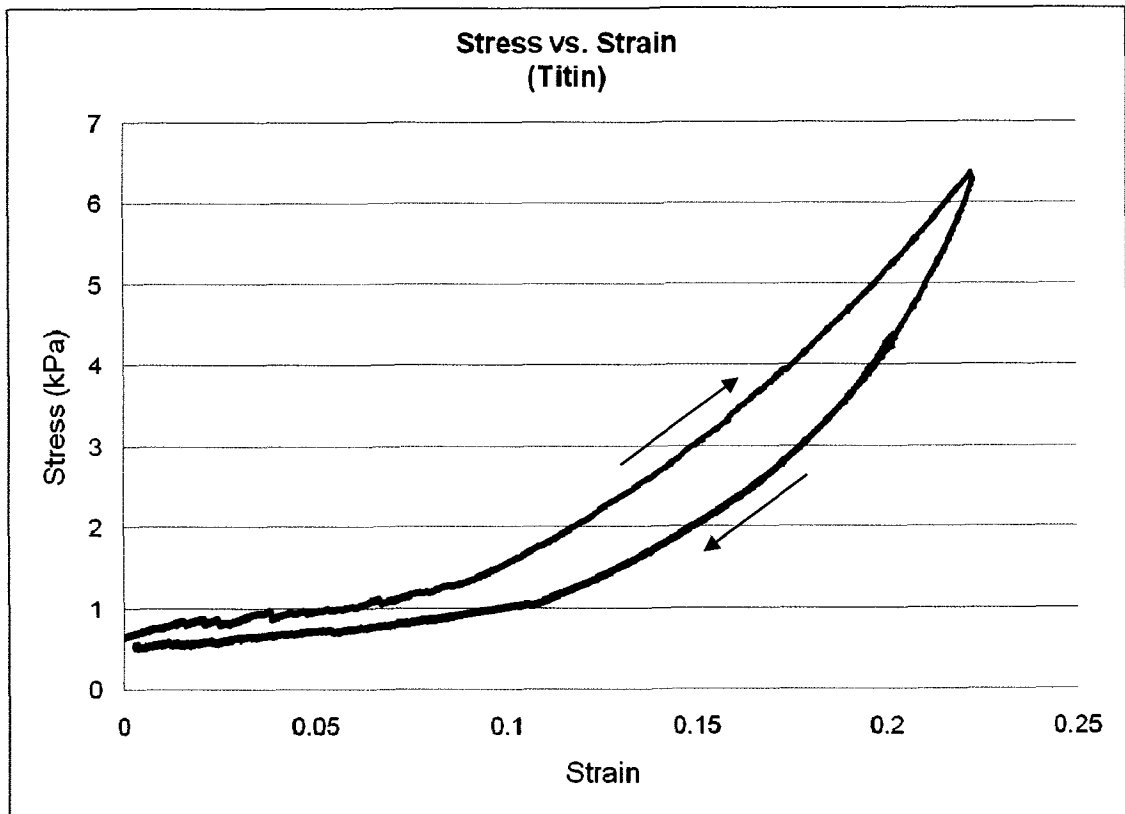
Figure 8.15 Stress – Strain Relationship; Contribution of Titin only.

It is clear from the shape of the graph in figure 8.15 that in presence of titin only, the muscle gets more stiffer at lower strain levels than that in case where only collagen is present. The hysteresis and maximum stress level at maximum subjected starin were also greater than those observed with presence of collagen only. Finally, we can conclude that the relative contribution of titin to the passive stiffness of this particular specimen was greater than that of collagen.

8.4 Saturation of Force Transducer

While performing experiments on other preparations, it was observed that many a times the passive force generated by the test specimen would go beyond 0.5mN, which was the capacity of the initially used force transducer. Hence there was loss of data from high strains. Figure 8.16 depicts the sudden flattening of the force curve whenever the force levels reached the maximum range of the force transducer.

The saturation of the force transducer called for immediate design modifications and hence the existing force transducer was replaced by one that had a maximum force measurement capacity of 10mN as stated in the design rationale. Tests have not yet been conducted with this particular device as a part of the experimental setup, but based on the theoretical and experimental data, the force transducer, with a higher range of measurement, is expected to serve well the research goals.
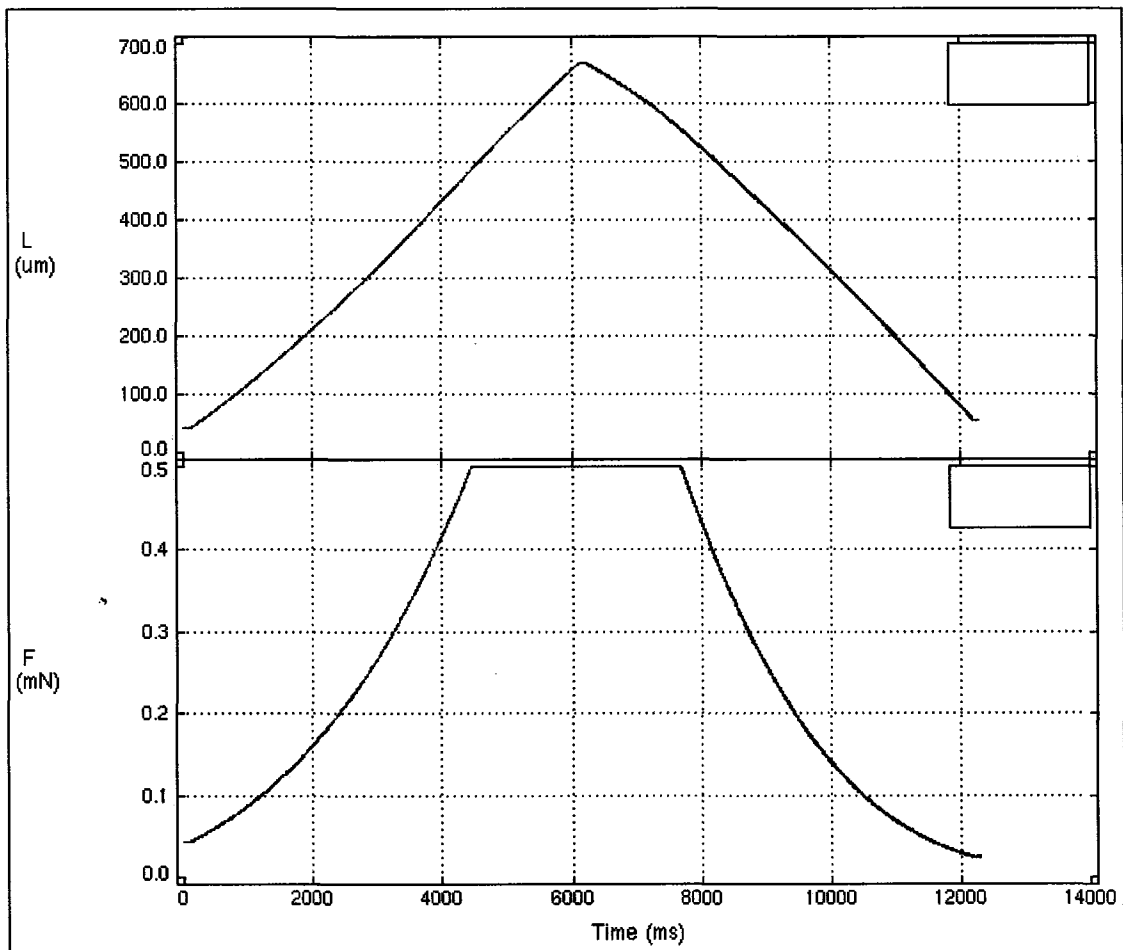
Figure 8.16 Force and Length Curves, Depicting Saturation of Force Transducer.

The specimen details that resulted in the graphs shown in figure 8.14 were as follows:

Animal	:	Pig
Tissue	:	Myocardium
Initial specimen length	:	2.82mm
Cross-sectional area	:	$0.071mm^2$
Sarcomere length	:	$1.91\mu m$
Subjected strain	:	23% (650μm)
Sampling frequency	:	10KHz

CHAPTER 9

DISCUSSION AND FUTURE WORK

9.1 Discussion

The primary aim of this thesis was to develop an experimental system – based on rational design principles – that could perform uniaxial stress test on small strips of passive (i.e., non-contracting) myocardium. The preliminary data obtained using this system indicates that a reliable system has been developed that would serve as the foundation for subsequent quantitative investigations of the contributions made by titin and collagen to the passive stiffness of myocardium.

Once the system was assembled and ready to be tested for suitability and reliability, tests were conducted with an intention of supporting as well as verifying the design rationale. The initial concept of the system, which targeted working with individual myocytes, was realized to be impractical from early investigations. This was mainly due to the infeasibility of isolating a single myocyte and attaching it to a mechanical test apparatus. Thus we decided to switch the goal to a system that would support investigations on a muscle strip rather than a single cell.

Preliminary results support the reliable nature of the re-designed system, once a force transducer with greater measurement capacity replaces the original one. The agreement of the preliminary stress-strain results with existing literature for typical rat myocardium supports the viability of the techniques. Once

supportive tests are conducted using this force transducer along with the fine tuning of the mounting, the system should be up and ready for real time experimentation.

9.2 Future Work

The next step to this research is testing the system, with higher measurement capacity force transducer system, to obtain data that prove the entirety of the setup to achieve data required to substantiate any hypothesis that would involve the usage of this experimental setup. In addition, a dynamic calibration technique would be developed to tackle the zero error encountered while collecting force related data. No solid ground work has yet been laid out for this, but this is one task that would soon require attention.

Further, the difficulties with fiber dissection technique shall be addressed. With the existing dissection procedure it is difficult to maintain sarcomeres oriented parallel to the axis of the muscle preparation. Sarcomeric orientation is essential to achieve effective stretch of the sarcomeres. Moreover, a preparation with uniform cross-sectional area with minimal damage around the outer edge of the specimen is more desirable. A healthy preparation is first step to achieving accurate data and hence refinement of the dissection procedure is highly important.

In addition to the dissection process, the methodology to attach clips to the specimen would also be revisited. At present, the most difficult task is to attach clips to the myocardial strip so that the axis of orientation of the strip is

maintained parallel to and through the center of the clips. If the clips are effectively attached, in a proper manner, to the specimen then the mounting procedure should become much easier.

A procedure would be developed to effectively mount the specimen onto the system and a have a common starting point, for all experiments, in terms of initial sarcomere length and force generated by the myocardial strip at rest state. The method of determination of unstressed specimen length being currently employed is fairly reproducible but needs to be improvised further. This process, once the calibration of force transducer is figured out, shall be more dependent on the control systems that we have.

While improving on the muscle preparation process and the image processing technique, we intend to attain more accurate sarcomere length measurements. Also, technique is being developed to measure the diameter of the specimen in two perpendicular directions, one of which can and is being measured as mentioned in the previous chapter. For the other direction, the plan is to shine light onto the preparation from the sideways instead of throwing light from the top, as in the inverted microscope. The light, as passing through the specimen, shall then be bent with the help of prism(s) in the direction of the lens system of the microscope to view or capture images. In fact, this method has been tried out a few times but the liquid medium in the bath slide poses a challenge of light being refraction when it enters the prism from the liquid medium.

The XY translation of the force transducer and the piezoelectric translation stage needs to be re-designed. At present, we face the problem of independent simultaneous displacement at both ends that translates the specimen while changing its length and orientation to the horizontal axis. In order to achieve synchronized motion that would allow us to translate the specimen without changing its length or the axis orientation, the manual translation stages will have to be replaced by motorized translation stages. Currently, synchronized motion in the Z direction is possible with the help of motorized translation stage at each end.

APPENDIX A

DEVICE TECHNICAL SPECIFICATIONS

A.1 Force Transducer

General Specifications

Operating temperature	:	0 to 40°C
Linearity of Output	:	±1% of full scale over full scale.
		±0.2% of full scale over 50% of full scale.
Power Requirements	:	120±10% VAC, 50/60 Hz, 20 W, maximum.

A.1.1 Technical Specifications for Model # 406A

Full scale	:	±0.5 mN
Sensitivity	:	0.05 mN/Volt
Resolution	:	0.01 μN
Step response time	:	5.0 ms
Resonance frequency	:	100 Hz
Compliance	:	10.0 micron/mN
Zero drift	:	0.05 μN/degC
Gain Drift	:	0.01 %.degC
Hysteresis	:	0.01 %
Maximum overload force	:	20 mN
Output Tube Length	:	7.0 mm
Output Tube Diameter	:	1.0 mm

A.1.2 Technical Specifications for Model # 405A

Full scale	:	±10 mN
Sensitivity	:	1 mN/Volt
Resolution	:	0.2 µN
Step response time	:	1.0 ms
Resonance frequency	:	600 Hz
Compliance	:	1.0 micron/mN
Zero drift	:	1 µN/degC
Gain Drift	:	0.01 %.degC
Hysteresis	:	0.01 %
Maximum overload force	:	100 mN
Output Tube Length	:	7.0 mm
Output Tube Diameter	:	1.0 mm

A.2 Digital Controller

Personal Computer

Processor	:	2.8 GHz P4
RAM	:	256 MB
Hard Disk	:	40 GB
Floppy Disk	:	1.44 KB
USB Flash Disk	:	64 MB
Ethernet Card	:	10/100 Mbits/sec
Keyboard	:	101 key, PS2 type

Mouse	:	PS2 type, Microsoft compatible
Power Requirements	:	120/240 VAC ±10%, 50/60 Hz, 5 amps max.
Dimensions	:	30 cm wide x 32.5 cm deep x 7.8 cm high
Weight	:	4 kg

A/D Card

<u>Analog Input</u>

Number of Channels	:	8 differential
Resolution	:	16 bits (1 part in 65535 parts)
Maximum Sampling Rate	:	200,000 samples per second

<u>Analog Output</u>

Number of Channels	:	2
Resolution	:	16 bits (1 part in 65535 parts)
Maximum Output Rate	:	200,000 updates per second

<u>Digital Input/Output</u>

Number of Channels	:	40
Type	:	TTL
Interface	:	104 conductor ribbon cable
Dimensions	:	½ length, PCI Bus

Operating System

Type	:	Real-time Linux.
Interface	:	GUI (Windows-type).

A.3 Signal Interface

Input Connector Type	:	BNC – isolated, male
Number of A/D Inputs	:	8 differential - Length In, Force In, Aux 1-6
Number of D/A Outputs	:	2 - Length Out, Force Out
Digital I/O	:	2 Inputs - Trg In 1, Trg In 2
4 Outputs	:	Trg Out 1, Trg Out 2, Stimulator, Inhibit

A.4 Piezo Linear Stage (P-622.1CD)

Motion and Positioning

Integrated Sensor	:	Capacitive
Open loop travel	:	300 µm
Closed loop travel	:	250 µm
Open loop resolution	:	0.7 nm
Closed loop resolution	:	0.4 nm
Closed loop linearity	:	0.02 %
Repeatability	:	±1 nm

Mechanical Properties

Stiffness	:	0.2 N/µm
Resonant frequency	:	400 Hz Unloaded
		185 Hz @ 120 g
Load capacity	:	10 N
Lateral force	:	10 N

Drive Properties

Ceramic type	:	PICMA P – 885
Electrical capacitance	:	3.1 µF

Miscellaneous

Active axes	:	X
Operating temperature	:	-20 to 80 deg C
Material	:	Aluminum
Dimensions	:	50 x 50 x 15 mm
Mass	:	0.2 kg

A.5 Piezo Linear Stage (P-628.1CD)

Motion and Positioning

Integrated Sensor	:	Capacitive
Open loop travel	:	950 µm
Closed loop travel	:	800 µm
Open loop resolution	:	1.8 nm
Closed loop resolution	:	0.5 nm
Closed loop linearity	:	0.03 %
Repeatability	:	±10 nm
Pitch / yaw	:	±6 µrad

Mechanical Properties

Stiffness	:	0.12 N/µm
Resonant frequency	:	125 Hz Unloaded
		115 Hz @ 20 g
		90 Hz @ 120 g
Load capacity	:	10 N
Lateral force	:	10 N

Drive Properties

Ceramic type	:	PICMA P – 887
Electrical capacitance	:	19 µF

Miscellaneous

Active axes	:	X
Operating temperature	:	-20 to 80 deg C
Material	:	Aluminum
Dimensions	:	80 x 80 x 17 mm
Mass	:	0.38 kg

A.6 Piezo Amplifier / Servo Controller

Sensor

Servo characteristics	:	P-I (analog), notch filter
Sensor type	:	Capacitive

Amplifier

Control i/p voltage range	:	-2 to +12 V
Min. output voltage	:	-20 to 120 V
Peak output power	:	36 W
Average output power	:	12 W
Peak current	:	360 mA
Average current	:	120 mA
Current limitation	:	Short-circuit-proof
Noise, 0 to 100 kHz	:	4.0 mV_{rms}
Voltage gain	:	10 ±0.1
Input impedance	:	100 kΩ

Interfaces and operation

Interface / communication	:	RS-232, 20 bit ADC/DAC, 9.6 - 115.2 kBaud
Piezo connector	:	LEMO Sub-D special
Sensor connection	:	LEMO Sub-D special
Analog input	:	BNC
Sensor monitor socket	:	BNC
Controller network	:	up to 12 channels, parallel
Display	:	2 x 4½-digits, LED
DC Offset	:	10-turn pot., adds 0 to 10 V to Control In

Miscellaneous

Operating temperature	:	5 to 50 °C
Overheat protection	:	Deactivation at 85 °C
Dimensions	:	236 x 88 x 273 mm + handles
Mass	:	2.5 kg
Operating voltage	:	90-120 / 220-240 VAC, 50-60 Hz
Max. power consumption	:	50 W

A.7 Micro Translation Stage

Motion and positioning

Travel range	:	15 mm
Integrated sensor	:	Rotary encoder
Sensor resolution	:	2048 Cts./rev.
Design resolution	:	0.0069 µm
Min. incremental motion	:	0.05 µm
Backlash	:	2 µm
Unidirectional repeatability	:	0.1 µm
Pitch / Yaw	:	±150 µrad
Max. velocity	:	1.5 mm/s

Mechanical properties

Drive screw	:	Leadscrew
Thread pitch	:	0.4 mm

Gear ratio	:	28.44444:1
Max. load	:	30 N
Max. push / pull force	:	10 N
Max. holding force	:	10 N
Max. lateral force	:	10 N

Drive properties

Motor type	:	DC-motor, gearhead
Operating voltage	:	0 to ±12 V
Electrical power	:	1.75 W
Current consumption	:	320 mA

Miscellaneous

Operating temperature	:	-20 to +65 °C
Material	:	Al (black anodized)
Mass	:	0.4 kg

A.8 CCD Camera

Specifications

Active image pixels	:	640(H) X 480(V), Mono
Active image area	:	4.74 mm X 3.55 mm
Pixel size	:	7.4 µm
Video output	:	Digital

Camera interface	:	Base camera link
Data clock	:	40.0 MHz
Resolution	:	640 X 480 pixels max
Frame rate	:	210 fps
Shutter speed	:	1/50000 sec to 1/100 sec
Long integration	:	1/100 sec to 10 sec
Gamma correction	:	G=1.0
Black level offset	:	256 levels/output
Video gain	:	6-40 dB, 1024 steps/output
External trigger	:	Asynchronous
Hardware trigger	:	External, optically isolated
Software trigger	:	Frame-grabber, CC1
S/N ratio	:	60 dB
Strobe output	:	Active HIGH, for external light source
Lens Mount	:	C mount, 1/3" format
Operating Temperature	:	-5 to 50 C
Min. illumination	:	1.0 Lux
Dimensions	:	67 x 67 x 41 mm
Mass	:	280 g

A.9 Automatic Temperature Controller

Specifications

Maximum output voltage	:	12 VDC
Maximum output current	:	1.5 A
Minimum load resistance	:	8.0 Ω
Manual voltage range	:	0.0 to 12.0 VDC
Maximum power output	:	16 W into a 9 Ω load
Power requirements	:	200-260 VAC, 50/60 Hz
Power fuse	:	0.5 A Slo-Blo
Front panel recorder o/p	:	T1 (control), T2 (Monitor), BNC
Rear panel input	:	T2 thermistor (monitor)
Temperature range	:	Ambient to 50 °C
Meter Display	:	3.5 digit LED display of temperature or voltage
Enclosure	:	17.0 x 3.5 x 12 inch

APPENDIX B

TEST PROTOCOLS

B.1 Functions

Following are the functions that were the used for the programs that were written to conduct the stretch process of the muscle strips:

1. Data-Enable

2. Length-Ramp

3. Data-Disable

4. Stop

B.1.1 Function Description

1. Data-Enable

This function instructs the system to begin data collection at the specified time. Data-Enable requires no parameters.

2. Length-Ramp

The Length-Ramp function performs a ramp change in length as per the given parameters. This function requires two parameters: 1) the desired length (in μm, mm, Lo, volts) and 2) the ramp time (in ms, s). The protocols that have been used for our purposes have Length-Ramp functions with the desired length in μm and ramp time in ms.

3. Data-Disable

Works exactly opposite to the Data-Enable function. The Data-Disable function commands the system to stop any further collection of data. This function also does not require any parameters.

4. Stop

Just as the name suggests, Stop ends the test protocol.

B.2 SYNTAX

Each line of the program adheres to a specific syntax which is as follows:

Step Number   Time (in ms)   Function   Parameters (if applicable)

Apart from the syntax, each protocol has a specific user defined sampling rate that can be selected from the provided drop down list.

B.3 The Program Codes

Following are the various protocols that were used to stretch the muscle strip through a desired length.

B.3.1 200 Microns Stretch with 10 kHz Sampling Frequency

1	0.0	Data-Enable	
2	100.0	Length-Ramp	200 um 2000 ms
3	2200.0	Length-Ramp	0 um 2000 ms
4	4300.0	Data-Disable	
5	4400.0	Stop	

B.3.2 250 Microns Stretch with 10 kHz Sampling Frequency

1	0.0	Data-Enable	
2	100.0	Length-Ramp	250 um 2500 ms
3	2700.0	Length-Ramp	0 um 2500 ms
4	5300.0	Data-Disable	
5	5400.0	Stop	

B.3.3 300 Microns Stretch with 2 kHz Sampling Frequency

1	0.0	Data-Enable	
2	100.0	Length-Ramp	300 um 3000 ms
3	3200.0	Length-Ramp	0 um 3000 ms
4	6300.0	Data-Disable	
5	6400.0	Stop	

B.3.4 350 Microns Stretch with 2 kHz Sampling Frequency

1	0.0	Data-Enable	
2	100.0	Length-Ramp	350 um 3500 ms
3	3700.0	Length-Ramp	0 um 3500 ms
4	7300.0	Data-Disable	
5	7400.0	Stop	

B.3.5 400 Microns Stretch with 2 kHz Sampling Frequency

1	0.0	Data-Enable	
2	100.0	Length-Ramp	400 um 4000 ms
3	4200.0	Length-Ramp	0 um 4000 ms
4	8300.0	Data-Disable	
5	8400.0	Stop	

B.3.6 450 Microns Stretch with 2 kHz Sampling Frequency

1	0.0	Data-Enable	
2	100.0	Length-Ramp	450 um 4500 ms
3	4700.0	Length-Ramp	0 um 4500 ms
4	9300.0	Data-Disable	
5	9400.0	Stop	

B.3.7 500 Microns Stretch with 2 kHz Sampling Frequency

1	0.0	Data-Enable	
2	100.0	Length-Ramp	500 um 5000 ms
3	5200.0	Length-Ramp	0 um 5000 ms
4	10300.0	Data-Disable	
5	10400.0	Stop	

B.3.8 550 Microns Stretch with 2 kHz Sampling Frequency

1	0.0	Data-Enable	
2	100.0	Length-Ramp	550 um 5500 ms
3	5700.0	Length-Ramp	0 um 5500 ms
4	11300.0	Data-Disable	
5	11400.0	Stop	

B.3.9 600 Microns Stretch with 2 kHz Sampling Frequency

1	0.0	Data-Enable	
2	100.0	Length-Ramp	600 um 6000 ms
3	6200.0	Length-Ramp	0 um 6000 ms
4	12300.0	Data-Disable	
5	12400.0	Stop	

B.3.10 650 Microns Stretch with 2 kHz Sampling Frequency

1	0.0	Data-Enable	
2	100.0	Length-Ramp	650 um 6500 ms
3	6700.0	Length-Ramp	0 um 6500 ms
4	13300.0	Data-Disable	
5	13400.0	Stop	

B.3.11 700 Microns Stretch with 2 kHz Sampling Frequency

1	0.0	Data-Enable	
2	100.0	Length-Ramp	700 um 7000 ms
3	7200.0	Length-Ramp	0 um 7000 ms
4	14300.0	Data-Disable	
5	14400.0	Stop	

B.3.12 750 Microns Stretch with 2 kHz Sampling Frequency

1	0.0	Data-Enable	
2	100.0	Length-Ramp	750 um 7500 ms
3	7700.0	Length-Ramp	0 um 7500 ms
4	15300.0	Data-Disable	
5	15400.0	Stop	

B.3.13 800 Microns Stretch with 2 kHz Sampling Frequency

1	0.0	Data-Enable	
2	100.0	Length-Ramp	800 um 8000 ms
3	8200.0	Length-Ramp	0 um 8000 ms
4	16300.0	Data-Disable	
5	16400.0	Stop	

B.4 Codes with Time Delay between Ramps

Programs were written to accommodate a 4second delay between consecutive ramp functions that allowed us to capture frames of the stretched sarcomere.

B.4.1 200 microns stretch with 10 KHz sampling frequency

1	0.0	Data-Enable	
2	100.0	Length-Ramp	200 um 2000 ms
3	6200.0	Length-Ramp	0 um 2000 ms
4	8300.0	Data-Disable	
5	8400.0	Stop	

B.4.2 250 microns stretch with 10 KHz sampling frequency

1	0.0	Data-Enable	
2	100.0	Length-Ramp	250 um 2500 ms
3	6700.0	Length-Ramp	0 um 2500 ms
4	9300.0	Data-Disable	
5	9400.0	Stop	

B.4.3 300 Microns Stretch with 2 kHz Sampling Frequency

1	0.0	Data-Enable	
2	100.0	Length-Ramp	300 um 3000 ms
3	7200.0	Length-Ramp	0 um 3000 ms
4	10300.0	Data-Disable	
5	10400.0	Stop	

B.4.4 350 Microns Stretch with 2 kHz Sampling Frequency

1	0.0	Data-Enable	
2	100.0	Length-Ramp	350 um 3500 ms
3	7700.0	Length-Ramp	0 um 3500 ms
4	11300.0	Data-Disable	
5	11400.0	Stop	

B.4.5 400 Microns Stretch with 2 kHz Sampling Frequency

1	0.0	Data-Enable	
2	100.0	Length-Ramp	400 um 4000 ms
3	8200.0	Length-Ramp	0 um 4000 ms
4	12300.0	Data-Disable	
5	12400.0	Stop	

B.4.6 450 Microns Stretch with 2 kHz Sampling Frequency

1	0.0	Data-Enable	
2	100.0	Length-Ramp	450 um 4500 ms
3	8700.0	Length-Ramp	0 um 4500 ms
4	13300.0	Data-Disable	
5	13400.0	Stop	

B.4.7 500 Microns Stretch with 2 kHz Sampling Frequency

1	0.0	Data-Enable	
2	100.0	Length-Ramp	500 um 5000 ms
3	9200.0	Length-Ramp	0 um 5000 ms
4	14300.0	Data-Disable	
5	14400.0	Stop	

B.4.8 550 Microns Stretch with 2 kHz Sampling Frequency

1	0.0	Data-Enable	
2	100.0	Length-Ramp	550 um 5500 ms
3	9700.0	Length-Ramp	0 um 5500 ms
4	15300.0	Data-Disable	
5	15400.0	Stop	

B.4.9 600 Microns Stretch with 2 kHz Sampling Frequency

1	0.0	Data-Enable	
2	100.0	Length-Ramp	600 um 6000 ms
3	10200.0	Length-Ramp	0 um 6000 ms
4	16300.0	Data-Disable	
5	16400.0	Stop	

B.4.10 650 Microns Stretch with 2 kHz Sampling Frequency

1	0.0	Data-Enable	
2	100.0	Length-Ramp	650 um 6500 ms
3	10700.0	Length-Ramp	0 um 6500 ms
4	17300.0	Data-Disable	
5	17400.0	Stop	

B.4.11 700 Microns Stretch with 2 kHz Sampling Frequency

1	0.0	Data-Enable	
2	100.0	Length-Ramp	700 um 7000 ms
3	11200.0	Length-Ramp	0 um 7000 ms
4	18300.0	Data-Disable	
5	18400.0	Stop	

B.4.12 750 Microns Stretch with 2 kHz Sampling Frequency

1	0.0	Data-Enable	
2	100.0	Length-Ramp	750 um 7500 ms
3	11700.0	Length-Ramp	0 um 7500 ms
4	19300.0	Data-Disable	
5	19400.0	Stop	

B.4.13 800 Microns Stretch with 2 kHz Sampling Frequency

1	0.0	Data-Enable	
2	100.0	Length-Ramp	800 um 8000 ms
3	12200.0	Length-Ramp	0 um 8000 ms
4	20300.0	Data-Disable	
5	20400.0	Stop	

APPENDIX C

SOLUTIONS COMPOSITION

C.1 Relaxing Solution

The following table list the reagents required to prepare the relaxing solution. Table C.2 gives the reagents that were added fresh to the relaxing solution as and when needed.

Table C.1 Reagents Used to Prepare Relaxing Solution.

Name	Molarity (mM)	Molar Mass (g/mol)	Volume (l)	Weight (mg)
EGTA	10	380.35	0.5	1901.75
KProp	80	112.16	0.5	4486.4
MgAc	6.4	214.4	0.5	686.08
NaATP	5.9	573.1	0.5	1690.645
BES	50	213.3	0.5	5332.5
NaN3	10	65.01	0.5	325.05
Creat-P	10	211.11	0.5	1055.55
DTT	1	154.25	0.5	77.125
Imidaz	40	68.08	0.5	1361.6

Table C.2 Reagents Added Fresh to the Relaxing Solution at the Time of Use.

Name	Molarity (mM)	Molar Mass (g/mol)	Volume (l)	Weight (mg)
PMSF	0.5	174.19	1	87.095
Leupeptin	0.04	463	1	18.52
BDM	20	101.1	1	2022

C.2 Depolymerizing Solutions

Two deplomerizing solutions were used to depolymerize the titin present in the sarcomeres in order to realize the effect of collagen only on the passive stiffness of the myocardium. Table C.3 list the details of the depolymerizing solutions used.

Table C.3 Depolymerizing Solutions Used to Depolymerize Titin.

Name	Molarity (mM)	Molar Mass (g/mol)	Volume (l)	Weight (mg)
KCl	600	74.551	0.005	223.653
KI	1000	166	0.005	830

APPENDIX D

PARAMETERS FOR USER DEFINED SCALE WITH IMAGE J

This section lists the various parametric values required for the user defined scales, on the basis of magnification factor of the objective, used to measure the sarcomere length.

Scale parameters for 1X objective:

Distance in pixels	:	0.140
Known Distance	:	1
Pixel Aspect Ratio	:	1
Unit of Length	:	µm
Scale	:	0.140 pixels/µm

Scale parameters for 5X objective:

Distance in pixels	:	0.680
Known Distance	:	1
Pixel Aspect Ratio	:	1
Unit of Length	:	µm
Scale	:	0.680 pixels/µm

Scale parameters for 10X objective:

Distance in pixels	:	1.360
Known Distance	:	1
Pixel Aspect Ratio	:	1
Unit of Length	:	µm
Scale	:	1.360 pixels/µm

Scale parameters for 40X objective:

Distance in pixels	:	5.340
Known Distance	:	1
Pixel Aspect Ratio	:	1
Unit of Length	:	µm
Scale	:	5.340 pixels/µm

REFERENCES

[1]   E. G. Lakatta and S. J. Sollott, "Perspectives on mammalian cardiovascular aging: humans to molecules," *Comparative Biochemistry and Physiology, Part A,* vol. 132, pp. 699-721, 2002.

[2]   D. A. Kass, J. G. F. Bronzwaer, and W. J. Paulus, "What mechanisms underlie diastolic dysfunction in heart failure?," *Circulation Research,* vol. 94, pp. 1533-1542, 2004.

[3]   M. R. Zile and D. L. Brutsaert, "New concepts in diastolic dysfunction and diastolic heart failure: part I diagnosis, prognosis, and measurements of diastolic function," *Circulation,* vol. 105, pp. 1387-1393, 2002.

[4]   M. R. Zile and D. L. Brutsaert, "New concepts in diastolic dysfunction and diastolic heart failure: part II causal mechanisms and treatment," *Circulation,* vol. 105, pp. 1503-1508, 2002.

[5]   E. G. Lakatta, "Arterial and cardiac aging: major shareholders in cardiovascular disease enterprises part III: cellular and molecular clues to heart and arterial aging," *Circulation,* vol. 107, pp. 490-497, 2003.

[6]   E. G. Lakatta and D. Levy, "Arterial and Cardiac Aging: Major Shareholders in Cardiovascular Disease Enterprises Part I: Aging Arteries: A "Set Up" for Vascular Disease," *Circulation,* vol. 107, pp. 139-146, 2003.

[7]   E. G. Lakatta and D. Levy, "Arterial and Cardiac Aging: Major Shareholders in Cardiovascular Disease Enterprises Part II: The Aging Heart in Health: Links to Heart Disease," *Circulation,* vol. 107, pp. 346-354, 2003.

[8]   J. W. Covell, "Factors influencing diastolic function. Possible role of the extracellular matrix," *Circulation,* vol. 81, p. 8, 1990.

[9]   S. Hein, S. Kostin, A. Heling, Y. Maeno, and J. Schaper, "The role of the cytoskeleton in heart failure," *Cardiovascular Research,* vol. 45, p. 273, 2000.

[10]   O. Cazorla, A. Freiburg, M. Helmes, T. Centner, M. McNabb, Y. Wu, K. Trombitas, S. Labeit, and H. Granzier, "Differential Expression of Cardiac Titin Isoforms and Modulation of Cellular Stiffness," *Circ Res,* vol. 86, pp. 59-67, 2000.

[11]   K. Trombitas, Y. Wu, D. Labeit, S. Labeit, and H. Granzier, "Cardiac titin isoforms are coexpressed in the half-sarcomere and extend independently," *American Journal of Physiology- Heart and Circulatory Physiology,* vol. 281, pp. 1793-1799, 2001.

[12]   H. Granzier, M. Helmes, O. Cazorla, M. McNabb, D. Labeit, Y. Wu, R. Yamasaki, A. Redkar, M. Kellermayer, and S. Labeit, "Mechanical properties of titin isoforms," *Advances in Experimental Medicine and Biology,* vol. 481, p. 283, 2000.

[13]   H. Granzier and S. Labeit, "Cardiac titin: an adjustable multi-functional spring," *J Physiol,* vol. 541, pp. 335-342, 2002.

[14]   K. Trombitas, A. Redkar, T. Centner, Y. Wu, S. Labeit, and H. Granzier, "Extensibility of isoforms of cardiac titin: variation in contour length of molecular subsegments provides a basis for cellular passive stiffness diversity," *Biophysical Journal,* vol. 79, pp. 3226-3234, 2000.

[15]   R. R. De Souza, "Aging of myocardial collagen," *Biogerontology,* vol. 3, pp. 325-335, 2002.

[16]   P. K. Mays, J. E. Bishop, and G. J. Laurent, "Age-related changes in the proportion of types I and III collagen," *Mechanisms of Ageing and Development,* vol. 45, pp. 203-212, 1988.

[17]   J. E. Bishop and G. J. Laurent, "Collagen turnover and its regulation in the normal and hypertrophying heart," *European Heart Journal,* vol. 16, pp. 38-44, 1995.

[18]   J. E. Bishop, S. Rhodes, G. J. Laurent, R. B. Low, and W. S. Stirewalt, "The regulation of collagen deposition in the hypertrophying heart," *Annals of the New York Academy of Sciences,* vol. 752, pp. 236-239, 1995.

[19]   D. Badenhorst, M. Maseko, O. J. Tsotetsi, A. Naidoo, R. Brooksbank, G. R. Norton, and A. J. Woodiwiss, "Cross-linking influences the impact of quantitative changes in myocardial collagen on cardiac stiffness and remodelling in hypertension in rats," *Cardiovascular Research,* vol. 57, pp. 632-641, 2003.

[20]   S. Kato, F. G. Spinale, R. Tanaka, W. Johnson, G. Cooper, and M. R. Zile, "Inhibition of collagen cross-linking: effects on fibrillar collagen and ventricular diastolic function," *American Journal of Physiology- Heart and Circulatory Physiology,* vol. 269, pp. 863-868, 1995.

[21] G. R. Norton, J. Tsotetsi, B. Trifunovic, C. Hartford, G. P. Candy, and A. J. Woodiwiss, "Myocardial stiffness is attributed to alterations in cross-linked collagen rather than total collagen or phenotypes in spontaneously hypertensive rats," *Circulation,* vol. 96, pp. 1991-1998, 1997.

[22] M. Asif, J. Egan, S. Vasan, G. Jyothirmayi, M. Masurekar, S. Lopez, C. Williams, R. Torres, D. Wagle, and P. Ulrich, "An advanced glycation endproduct cross-link breaker can reverse age-related increases in myocardial stiffness," *Proceedings of the National Academy of Sciences of the United States of America,* vol. 97, pp. 2809-2813, 2000.

[23] R. Candido, J. Forbes, M. Thomas, V. Thallas, R. Dean, W. Burns, C. Tikellis, R. Ritchie, S. Twigg, and M. Cooper, "A breaker of advanced glycation end products attenuates diabetes-induced myocardial structural changes," *Circ Res,* vol. 92, pp. 785-792, 2003.

[24] B. Corman, M. Duriez, P. Poitevin, D. Heudes, P. Bruneval, A. Tedgui, and B. Levy, "Aminoguanidine prevents age-related arterial stiffening and cardiac hypertrophy," *Proceedings of the National Academy of Sciences of the United States of America,* vol. 95, pp. 1301-1306, 1998.

[25] K. Herrmann, A. McCulloch, and J. Omens, "Glycated collagen cross-linking alters cardiac mechanics in volume-overload hypertrophy," *American Journal of Physiology- Heart and Circulatory Physiology,* vol. 284, pp. 1277-1284, 2003.

[26] D. Iimoto, J. Covell, and E. Harper, "Increase in cross-linking of type I and type III collagens associated with volume-overload hypertrophy," *Circulation Research,* vol. 63, pp. 399-408, 1988.

[27] G. Norton, G. Candy, and A. Woodiwiss, "Aminoguanidine prevents the decreased myocardial compliance produced by streptozotocin-induced diabetes mellitus in rats," *Circulation,* vol. 93, pp. 1905-1912, 1996.

[28] J. M. Ervasti, "Costameres: the Achilles' Heel of Herculean Muscle," *J. Biol. Chem.,* vol. 278, pp. 13591-13594, 2003.

[29] M. M. LeWinter, Y. Wu, S. Labeit, and H. Granzier, "Cardiac titin: Structure, functions and role in disease," *Clinica Chimica Acta,* vol. 375, pp. 1-9, 2007.

[30] H. L. Granzier and S. Labeit, "The Giant Protein Titin: A Major Player in Myocardial Mechanics, Signaling, and Disease," *Circ Res,* vol. 94, pp. 284-295, 2004.

[31]   E. H. Lee, J. Hsin, O. Mayans, and K. Schulten, "Secondary and Tertiary Structure Elasticity of Titin Z1Z2 and a Titin Chain Model," *Biophys. J.,* vol. 93, pp. 1719-1735, 2007.

[32]   S. Hein, W. H. Gaasch, and J. Schaper, "Giant Molecule Titin and Myocardial Stiffness," *Circulation,* vol. 106, pp. 1302-1304, 2002.

[33]   A. Freiburg, K. Trombitas, W. Hell, O. Cazorla, F. Fougerousse, T. Centner, B. Kolmerer, C. Witt, J. S. Beckmann, C. C. Gregorio, H. Granzier, and S. Labeit, "Series of Exon-Skipping Events in the Elastic Spring Region of Titin as the Structural Basis for Myofibrillar Elastic Diversity," *Circ Res,* vol. 86, pp. 1114-1121, 2000.

[34]   H. Granzier, D. Labeit, Y. Wu, and S. Labeit, "Section: The Elastic Vertebrate Muscle Protein Titin; Titin as a modular spring: emerging mechanisms for elasticity control by titin in cardiac physiology and pathophysiology," *Journal of Muscle Research and Cell Motility,* vol. 23, pp. 457-470, 2002.

[35]   H. L. Granzier and T. C. Irving, "Passive tension in cardiac muscle: contribution of collagen, titin, microtubules, and intermediate filaments," *Biophys. J.,* vol. 68, pp. 1027-1044, 1995.

[36]   S. P. Bell, L. Nyland, M. D. Tischler, M. McNabb, H. Granzier, and M. M. LeWinter, "Alterations in the Determinants of Diastolic Suction During Pacing Tachycardia," *Circ Res,* vol. 87, pp. 235-240, 2000.

[37]   S. F. Nagueh, G. Shah, Y. Wu, G. Torre-Amione, N. M. P. King, S. Lahmers, C. C. Witt, K. Becker, S. Labeit, and H. L. Granzier, "Altered Titin Expression, Myocardial Stiffness, and Left Ventricular Function in Patients With Dilated Cardiomyopathy," *Circulation,* vol. 110, pp. 155-162, 2004.

[38]   C. Neagoe, M. Kulke, F. del Monte, J. K. Gwathmey, P. P. de Tombe, R. J. Hajjar, and W. A. Linke, "Titin Isoform Switch in Ischemic Human Heart Disease," *Circulation,* vol. 106, pp. 1333-1341, 2002.

[39]   S. L. Thieszen and T. H. Rosenquist, "Expression of collagens and decorin during aortic arch artery development: implications for matrix pattern formation," *Matrix Biology,* vol. 14, pp. 573-582, 1995.

[40]   G. Montes, "Structural biology of the fibres of the collagenous and elastic systems," *Cell Biology International,* vol. 20, pp. 15-27, 1996.

[41] J. Ohayon and R. Chadwick, "Effects of collagen microstructure on the mechanics of the left ventricle," *Biophysical Journal,* vol. 54, pp. 1077-1088, 1988.

[42] J. Janicki and G. Brower, "The role of myocardial fibrillar collagen in ventricular remodeling and function," *Journal of Cardiac Failure,* vol. 8, pp. 319-325, 2002.

[43] T. Robinson, L. Cohen-Gould, and S. Factor, "Skeletal framework of mammalian heart muscle: arrangement of inter- and pericellular connective tissue structures," *Laboratory Investigation,* vol. 49, pp. 482-498, 1983.

[44] T. K. Borg and J. B. Caulfield, "The collagen matrix of the heart," *Fred Proc.,* vol.40, p. 2037-2041, 1981.

[45] J. B. Caulfield and T. K. Borg, "The collagen network of the heart," *Laboratory Investigation; A Journal of Technical Methods and Pathology,* vol. 40, p. 364, 1979.

[46] J. Capasso, T. Robinson, and P. Anversa, "Alterations in collagen cross-linking impair myocardial contractility in the mouse heart," *Circulation Research,* vol. 65, pp. 1657-1664, 1989.

[47] J. E. Bishop, "Regulation of cardiovascular collagen deposition by mechanical forces," *Molecular Medicine Today,* vol. 4, pp. 69-75, 1998.

[48] T. Borg, W. Ranson, F. Moslehy, and J. Caulfield, "Structural basis of ventricular stiffness," *Laboratory Investigation; A Journal of Technical Methods and Pathology,* vol. 44, p. 49, 1981.

[49] K. T. Weber, J. S. Janicki, R. Pick, C. Abrahams, S. G. Shroff, R. I. Bashey, and R. M. Chen, "Collagen in the hypertrophied, pressure-overloaded myocardium," *Circulation,* vol. 75, p. I40, 1987.

[50] S. M. Weis, J. L. Emery, K. D. Becker, D. J. McBride, Jr, J. H. Omens, and A. D. McCulloch, "Myocardial Mechanics and Collagen Structure in the Osteogenesis Imperfecta Murine (OIM)," *Circ Res,* vol. 87, pp. 663-669, 2000.

[51] M. L. Burgess, J. C. McCrea, and H. L. Hedrick, "Age-associated changes in cardiac matrix and integrins," *Mechanisms of Ageing and Development,* vol. 122, pp. 1739-1756, 2001.